General Disclaimer

One or more of the Following Statements may affect this Document

- This document has been reproduced from the best copy furnished by the organizational source. It is being released in the interest of making available as much information as possible.

- This document may contain data, which exceeds the sheet parameters. It was furnished in this condition by the organizational source and is the best copy available.

- This document may contain tone-on-tone or color graphs, charts and/or pictures, which have been reproduced in black and white.

- This document is paginated as submitted by the original source.

- Portions of this document are not fully legible due to the historical nature of some of the material. However, it is the best reproduction available from the original submission.

NASA TECHNICAL MEMORANDUM

NASA TM X- 73333
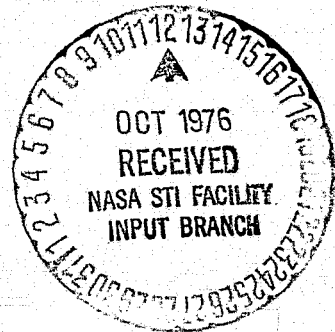
AN ANALYTICAL AND EXPERIMENTAL EVALUATION OF A FRESNEL LENS SOLAR CONCENTRATOR

By Leon J. Hastings, Steve A. Allums, and Dr. Ronald M. Cosby
Structures and Propulsion Laboratory

August 1976

OCT 1976
RECEIVED
NASA STI FACILITY
INPUT BRANCH

NASA

George C. Marshall Space Flight Center

Marshall Space Flight Center, Alabama

1. REPORT NO. NASA TM X-73333	2. GOVERNMENT ACCESSION NO.	3. RECIPIENT'S CATALOG NO.
4 TITLE AND SUBTITLE An Analytical and Experimental Evaluation of a Fresnel Lens Solar Concentrator		5. REPORT DATE August 1976
		6. PERFORMING ORGANIZATION CODE
7. AUTHOR(S) Leon J. Hastings, Steve A. Allums, and Dr. Ronald M. Cosby*		8. PERFORMING ORGANIZATION REPORT #
9. PERFORMING ORGANIZATION NAME AND ADDRESS George C. Marshall Space Flight Center Marshall Space Flight Center, Alabama 35812		10. WORK UNIT NO.
		11. CONTRACT OR GRANT NO.
		13. TYPE OF REPORT & PERIOD COVERED
12. SPONSORING AGENCY NAME AND ADDRESS National Aeronautics and Space Administration Washington, D.C. 20546		Technical Memorandum
		14. SPONSORING AGENCY CODE

15. SUPPLEMENTARY NOTES

Prepared by Structures and Propulsion Laboratory, Science and Engineering
* Ball State University

16. ABSTRACT

Plastic Fresnel lenses for solar concentration are attractive because of low cost, mass production potential. Therefore, an analytical and experimental evaluation of line-focusing Fresnel lenses with application potential in the 200° to 370°C range is in progress. Analytical techniques have been formulated to assess the solar transmission and imaging properties of a grooves-down lens. Experimentation was based on a 56 cm wide, f/1.0 lens. A Sun tracking heliostat provided a nonmoving solar source. Measured data indicated more spreading at the profile base than analytically predicted, resulting in a peak concentration 18 percent lower than the computed peak of 57. The measured and computed transmittances were 85 and 87 percent, respectively. Preliminary testing with a subsequent lens indicated that modified manufacturing techniques corrected the profile spreading problem and should enable improved analytical experimental correlation.

EDITOR'S NOTE

Use of trade names or names of manufacturers in this report does not constitute an official endorsement of such products or manufacturers, either expressed or implied, by the National Aeronautics and Space Administration or any other agency of the United States government.

17. KEY WORDS		18. DISTRIBUTION STATEMENT
		Unclassified — Unlimited

19. SECURITY CLASSIF. (of this report)	20. SECURITY CLASSIF. (of this page)	21. NO. OF PAGES	22. PRICE
Unclassified	Unclassified	52	NTIS

TABLE OF CONTENTS

LIST OF ILLUSTRATIONS

LIST OF ILLUSTRATIONS (Concluded)

NOMENCLATURE

Symbol	Definition
A	total transmitted fraction of incident sunlight
A_j	transmitted fraction of incident sunlight in jth wavelength interval
f	lens focal length
$H(\lambda), H_j$	solar intensity at wavelength λ_j or in jth wavelength interval
$I_{ij}(Y)$	intensity contribution from ith serration and jth wavelength interval
$I_j(Y)$	intensity at position Y due to incident solar flux within jth wavelength interval
$I(Y)$	total intensity at position Y
i	serration index
j	wavelength index
L, L_{ij}	beam spread for sunlight within jth wavelength interval refracted from ith serration
$\Delta \ell$	defocus length parameter
m, p	ray lens geometrical parameters
N	design index of refraction
n	index of refraction
q	incident solar intensity
q_j	incident solar intensity in jth wavelength interval

NOMENCLATURE (Continued)

Symbol	Definition
T_a	bulk transmittance factor
T_1, T_2	Fresnel transmittance factors for smooth and serrated lens surfaces, respectively
T, T_{ij}	transmittance through ith serration for sunlight within jth wavelength interval
$T_i(y)$	sunlight transmittance for ith serration
t	lens thickness
Δt	groove depth
W	lens width
y	distance from lens centerline
$(\Delta y)_i$	serration width
Y	position variable in image plane
Y_r, Y_ℓ	extreme ray intercepts
2α	apparent angular diameter of Sun
α'	extreme ray refraction angle at first lens surface
β	emergent ray/lens normal angle for incident light
β'	emergent ray/lens normal angle for incident light of the design wavelength
γ_a, γ_c	extreme emergent ray/lens normal angles

NOMENCLATURE (Concluded)

Symbol	Definition
ζ	linear groove density, lines/unit width
θ	groove angle
λ	wavelength
ω_j	solar flux weighting factor

AN ANALYTICAL AND EXPERIMENTAL EVALUATION OF A FRESNEL LENS SOLAR CONCENTRATOR

I. INTRODUCTION

Solar concentration activities at the Marshall Space Flight Center (MSFC) during the past year have centered on plastic, line-focusing Fresnel lenses which generate temperatures in the 200° to 370°C range [1]. Compared to other concentration concepts, the technique is relatively unexplored; however, the acrylic lens is adaptable to mass production techniques by casting and/or calendaring-extrusion processes which permit relatively low manufacturing costs [2]. The durability and weatherability of acrylic [3] and the ease of cleaning are other desirable qualities.

The suitability of acrylic lenses depends largely on optical transmission and imaging performance with respect to the solar source. The total required collector area for a given application is a function of lens transmittance. The design of a collection tube assembly to intercept the concentrated flux is subject to the intensity distribution of concentrated radiation beneath the lens. Size and complexity of support structure and tracking mechanisms depend on the lens f-number which, in turn, must be optimized with respect to the optical properties.

Based on this background, the optical performance of Fresnel lens solar concentrators is being investigated analytically and experimentally. The analytical effort reported herein extends an earlier study [4] of a perfectly tracking lens to include the intensity distribution across the solar spectrum, the index of refraction variation with wavelength, and defocusing effects. Simple ray optics and the laws of reflection and refraction were used to develop theoretical expressions for transmittance and for the distribution of concentrated sunlight. The experimentation was performed using a 56 cm wide acrylic lens with f-number of one. A major objective was to measure the sensitivity of the lens transmission and concentration characteristics with respect to Sun alignment errors and defocusing.

These analytical and experimental evaluations have been performed
in support of and in preparation for testing with a 1.83 by 3.66 m (6 by 12 ft)
lens collector assembly. Testing with this large scale collector was initiated
in July 1976 and results will be reported at a later date.

II. THEORY

A. Background

A cylindrical Fresnel lens basically consists of a thin sheet of refracting
material with linear serrations or grooves on one surface. The groove angles
are selected such that all incident parallel rays of light of a chosen wavelength
intercepted by the lens are focused to a common focal line. Fresnel concentra-
tors can be designed for utilization in either of two modes: (1) grooved surface
toward the Sun (grooves-up), (2) grooves away from the Sun (grooves-down).
A "grooves-down" geometry is sketched in Figure 1. The "grooves-up" and
grooves-down versions were previously evaluated using an initial analytical
model [4]. The grooves-up configuration provided better concentration, but at
the expense of a lower transmittance. The disadvantages of groove exposure to
dust and other contaminants were concluded to outweigh the advantages of the

Figure 1. Grooves-down cylindrical Fresnel lens.

These analytical and experimental evaluations have been performed in support of and in preparation for testing with a 1.83 by 3.66 m (6 by 12 ft) lens collector assembly. Testing with this large scale collector was initiated in July 1976 and results will be reported at a later date.

II. THEORY

A. Background

A cylindrical Fresnel lens basically consists of a thin sheet of refracting material with linear serrations or grooves on one surface. The groove angles are selected such that all incident parallel rays of light of a chosen wavelength intercepted by the lens are focused to a common focal line. Fresnel concentrators can be designed for utilization in either of two modes: (1) grooved surface toward the Sun (grooves-up), (2) grooves away from the Sun (grooves-down). A "grooves-down" geometry is sketched in Figure 1. The "grooves-up" and grooves-down versions were previously evaluated using an initial analytical model [4]. The grooves-up configuration provided better concentration, but at the expense of a lower transmittance. The disadvantages of groove exposure to dust and other contaminants were concluded to outweigh the advantages of the
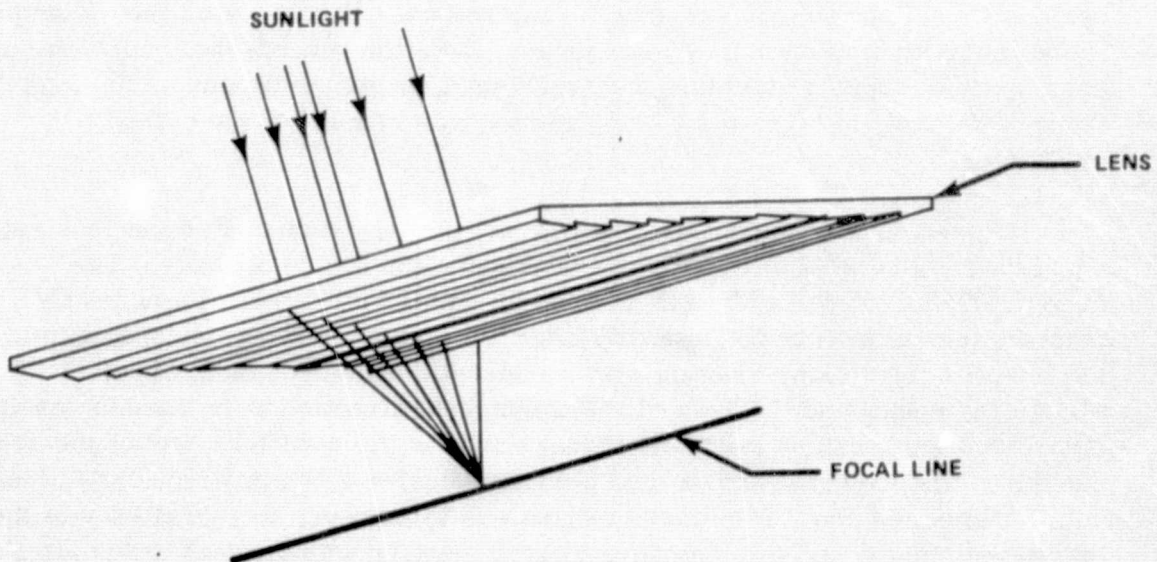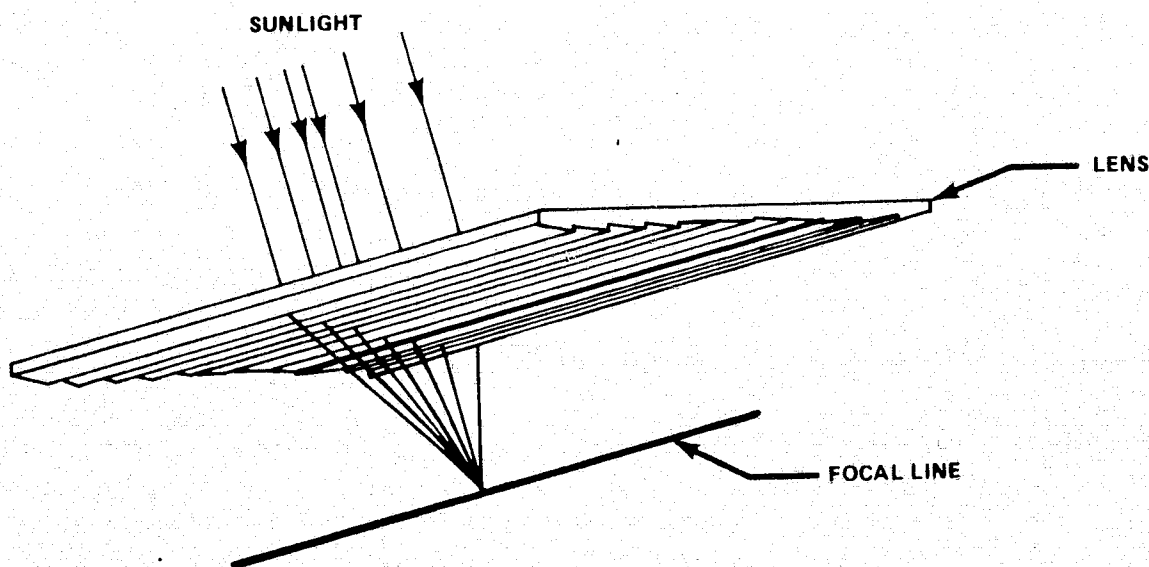
Figure 1. Grooves-down cylindrical Fresnel lens.

grooves-up geometry; therefore, the grooves-down configuration was baselined for further assessment. Furthermore, performance sensitivity studies indicated that an f-number of one (f/1.0) was optimum from a transmittance and concentration profile standpoint. The current theoretical model and further results concerning an f/1.0 grooves-down lens are described in subsequent sections.

B. Model Assumptions

Development of the ray trace model was based on a perfectly tracking lens with a compression-molded type geometry. Lens manufacturing defects and deflection due to wind loads and thermal expansion/contraction were neglected. Additional model assumptions were:

1. The solar flux refracted by a single serration is uniformly distributed over the beam spread width in the intercept plane beneath the lens.

2. The Sun is a uniform source of radiation, i.e., all points on the solar disc are assumed to have equal energy emission rates.

3. The depth of a lens serration is negligible compared to the focal length.

4. Diffraction effects are negligible.

5. No anomalous dispersion effects near absorption bands in the lens material occur.

C. Groove Angles

The groove angle corresponding to a design index of refraction (N) can be determined by referring to the ray diagram in Figure 2(a). Using Snell's law of refraction,

$$N \sin \theta = \sin(\beta' + \theta) \tag{1}$$

where θ is the groove angle and β' is the refracted ray angle relative to the lens surface normal for a design wavelength ray. Further,
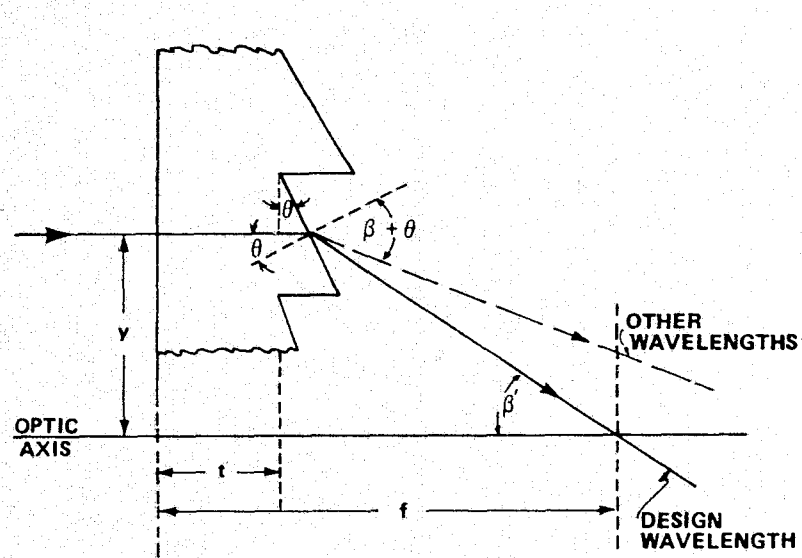
(a) COLLIMATED LIGHT SOURCE   (b) SOLAR SOURCE
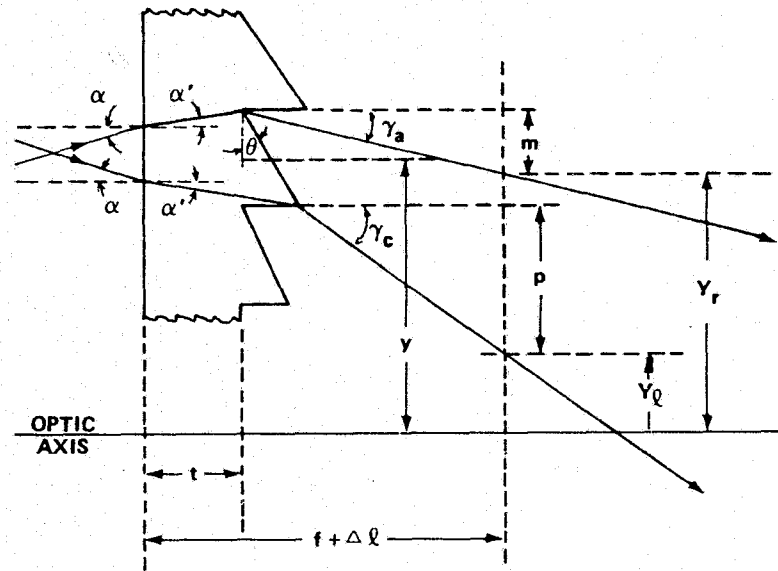
Figure 2. Ray diagrams for Fresnel lens solar concentrator.

$$\tan \beta' \simeq \frac{y}{f - t} \tag{2}$$

where y is the serration distance from the lens axis, f is the focal length, and t the lens center thickness.

Combining equations (1) and (2),

$$\theta = \text{Arc tan} \left[\frac{y}{N[y^2 + (f - t)^2]^{1/2} - (f - t)} \right] \tag{3}$$

where the assumption that the groove depth $\Delta t \ll f - t$ is used. For a given design index of refraction and focal length, equation (3) yields the groove angle as a function of serration position.

D. Transmission Characteristics

1. <u>Transmission Coefficient</u>. Transmission losses occur primarily through reflection and absorption. Reflection losses at the lens air-plastic boundaries are analyzed using the Fresnel formulae to calculate the transmittance of each surface for incident parallel light of a given wavelength [4,5]. The attenuation of solar flux by absorption in the infrared (IR) and ultraviolet (UV) of the spectrum is empirically modeled.

The transmission coefficient is the product of Fresnel transmittance factors T_1 and T_2 for the first and second lens surfaces, respectively, and a bulk transmittance factor T_a, i.e.,

$$T = T_1 T_2 T_a \quad . \tag{4}$$

Rays from the solar source extremities deviate from the lens optical axis by only approximately 16 min of arc. Thus, it is sufficient to determine the product $T_1 T_2$ for parallel rays only. Referring to Figure 2, light of a wavelength other than the design wavelength emerges from the lens at an angle β with respect to the axis (rather than β'). Using Snell's law,

$$\beta = \text{Arc sin} (n \sin \theta) - \theta \quad , \tag{5}$$

5

where n is the index of refraction for the particular wavelength chosen.

As shown in Reference 4, the Fresnel formulae can be used to derive the relation:

$$T_1 T_2 = \frac{2n(1 + \cos^2 \beta) \sin 2\theta \sin 2(\beta + \theta)}{(n+1)^2 \cos^2 \beta \sin^2 (\beta + 2\theta)} \qquad . \tag{6}$$

The bulk transmittance factor is empirically determined assuming the bulk transmittance at normal incidence is also applicable within the range of incident angles considered. For a given wavelength interval, data such as in Figure 3 can be used to establish the actual average transmittance through the lens material for normal incidence. Because the calculated transmittance at normal incidence, assuming reflection losses only, is

$$T_1 T_2 = \frac{16n^2}{(n+1)^2} \qquad , \tag{7}$$

then the bulk transmittance can be computed using the relation

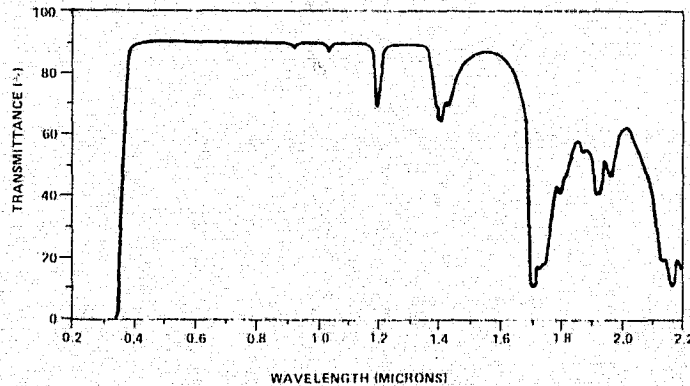$$T_a = \frac{T \text{ (measured)}}{\dfrac{16n^2}{(n+1)^2}} \qquad . \tag{8}$$

Figure 3. Plexiglas molding powder transmittance.

This factor is then used in equation (4) when determining the transmission coefficient for each serration and wavelength increment of the solar spectrum.

It should be noted that the complicated, but fundamentally more correct, approach to the problem of analyzing absorption would involve rederiving the Fresnel formulae with the index of refraction taken to be a complex number.

2. <u>Total Lens Transmittance.</u> To determine the total fraction of incident sunlight transmitted through the lens, the variation of sunlight intensity with wavelength must be considered. The total solar flux q, i.e., energy per unit area per unit time is

$$q = \int_0^\infty H(\lambda) \, d\lambda \qquad , \qquad (9)$$

where $H(\lambda)$ is the solar intensity at wavelength λ, or approximately

$$q = \sum_j q_j = \sum_j H_j (\Delta\lambda)_j \qquad . \qquad (10)$$

Defining

$$q_j \equiv \omega_j q \qquad , \qquad (11)$$

the weighting factor is

$$\omega_j = \frac{H_j(\Delta\lambda)_j}{q} = \frac{H_j(\Delta\lambda)_j}{\sum_j H_j(\Delta\lambda)_j} \qquad . \qquad (12)$$

Obviously,

$$\sum_j \omega_j = 1 \qquad . \qquad (13)$$

The total energy per unit time per unit length transmitted through one serration, the ith, is obtained by summing contributions from all wavelength intervals within the solar spectrum, i.e.,

$$\text{transmitted energy} = \sum_j T_{ij} \, q_j (\Delta y)_i \qquad , \tag{14}$$

where the transmissivity is given by equation (4) and $(\Delta y)_i$ is the serration width. The serration transmission as a function of serration position is then

$$T_i(y) = \frac{\sum_j T_{ij} \, q_j (\Delta y)_i}{q(\Delta y)_i} \quad . \tag{15}$$

Using equation (11),

$$T_i(y) = \sum_j \omega_j \, T_{ij}(y) \quad . \tag{16}$$

By summing overall serrations $\sum_i'$, the total energy per unit time per unit length through the lens is

$$\text{total transmitted energy} = \sum_i' \sum_j' T_{ij} \, q_j (\Delta y)_i \quad . \tag{17}$$

The total fraction, A, of incident solar energy transmitted is

$$A = \frac{\sum_i' \sum_j' T_{ij} \, q_j (\Delta y)_i}{\sum_i' \sum_j' q_j (\Delta y)_i} \quad . \tag{18}$$

Using equation (11),

8

$$A = \frac{2}{W} \sum_i \sum_j T_{ij} \, \omega_j (\Delta y)_i \qquad , \qquad (19)$$

where the summation is over one half the lens and W is the lens width.

If a constant groove spacing, ζ, is assumed, then

$$A = \frac{2}{\zeta W} \sum_i \sum_j T_{ij} \, \omega_j = \sum_j \omega_j A_j \qquad , \qquad (20)$$

where A_j is the fraction of incident light transmitted for one wavelength interval.

E. Concentrated Flux Distribution

The intensity profile of concentrated sunlight beneath the lens can be determined by recalling model assumption number 1 of Section II.B. and referring to Figure 2(b). Because the intensity will not be a function of distance along the lens length axis, the problem reduces to a one-dimensional determination of the intensity profile. Defining L_{ij} as the beam spread width in a chosen plane beneath the concentrator, the intensity contribution at distance +Y from the optical axis from sunlight with wavelength λ_j refracted by the ith serration is

$$I_{ij}(Y) = \frac{T_{ij} \, q_j (\Delta y)_i}{L_{ij}} \qquad . \qquad (21)$$

The local concentration ratio due to the jth wavelength segment of the solar spectrum results when the contributions from all serrations are summed:

$$\frac{I_j(Y)}{q} = \omega_j \sum_j \frac{T_{ij}(\Delta y)_i}{L_{ij}} \qquad . \qquad (22)$$

The sum of the contributions from each wavelength segment of the solar spectrum then yields the total local concentration ratio:

$$\frac{I(Y)}{q} = \sum_j \frac{I_j(Y)}{q} = \sum_j \sum_i \frac{\omega_j \, T_{ij} \, (\Delta y)_i}{L_{ij}} \qquad . \tag{23}$$

To determine the local concentration ratio at any position, Y, the beam spread for each wavelength and each serration must be calculated. The rays determining the beam spread are the extreme rays (Y_r and Y_ℓ) refracted and exiting at the edges of individual serrations.

Referring to Figure 2(b),

$$L = Y_r - Y_\ell \tag{24}$$

$$Y_r = y + \left(\frac{\Delta y}{2}\right) - m \tag{25}$$

and

$$Y_\ell = y - \left(\frac{\Delta y}{2}\right) - p \qquad . \tag{26}$$

Now, from the geometry present, it is evident that

$$m = (f + \Delta \ell - t) \tan \gamma_a \tag{27}$$

and

$$p = (f + \Delta \ell - t - \Delta y \tan \theta) \tan \gamma_c \qquad , \tag{28}$$

where $\Delta \ell$ is the "defocus parameter" and γ_a and γ_c are exit angles for the refracted rays.

10

From Snell's law for refraction, γ_a and γ_c are determined:

$$\gamma_a = \text{Arc} \sin[n \sin(\theta - \alpha')] - \theta \tag{29}$$

$$\gamma_c = \text{Arc} \sin[n \sin(\theta + \alpha')] - \theta \quad , \tag{30}$$

where

$$\alpha' = \text{Arc} \sin\left(\frac{\sin \alpha}{n}\right) \quad , \tag{31}$$

and 2α is the angle subtended by the solar disc.

Equations (24) through (31) suffice to determine the beam spread, L, and corresponding intercepts for a given serration and wavelength. Because the transmission coefficient has previously been determined, the desired intensity profiles can be calculated from equation (23) if proper weighting factors and indices of refraction are selected for the chosen wavelength intervals.

III. THEORETICAL RESULTS

A computer program based on the preceding theory has been used to develop example performance data for a cylindrical Fresnel lens. Detailed parameter study results concerning the effects of f-number on serration geometry, transmission coefficient, focal plane target width, and focused solar flux distribution are presented in Reference 4 for a single wavelength, 5893 Å. Therefore, the data presented herein were selected to extend the previous f/1.0 lens study results to include the influence of refractive variation with wavelength and of defocusing the target plane. Additional parameters were selected to correspond with an existing lens that was used in the experimental evaluation (Table 1).

The sea level solar spectral distribution defined by the extensive numerical data in Table III of Parry Moon's "Proposed Standard Solar Radiation Curves for Engineering Use" [6] was utilized as baseline input in the wavelength effect

TABLE 1. TEST LENS CHARACTERISTICS

Lens Type	Cylindrical Fresnel, Grooves-Down
Material	Rohm and Haas Plexiglas VS
Fabrication Technique	Compression Molding
Manufacturer	Optical Sciences Group
Width	56 cm (22 in.)
f-number	1.0
Center Thickness	0.434 cm (0.171 in.)
Groove Density	13.58/cm (34.5/in.)
Design Wavelength	5893 Å

calculations. By considering the fraction of the solar constant in the wavelength range from 0 to λ as a function of λ (Fig. 4), the previously discussed weighting factors for selected wavelength intervals could be determined (Table 2). Appropriate indices of refraction for acrylic and the bulk transmittance factors (T_a) were defined using manufacturer's data [7].

Analytical results describing wavelength and defocusing influences on lens transmittance and concentration characteristics are presented in the following material. Such data can, in turn, be utilized to estimate lens collector area requirements for various applications and in the design and placement of collection tube assemblies beneath lens.

A. Lens Transmittance

Transmission losses by reflection and wavelength effects were assessed using equation (6). The results are illustrated in Figure 5 which presents the product T_1T_2 versus serration position for two wavelengths, 4000 Å and 15 260 Å. These wavelengths represent the near UV and IR extremes
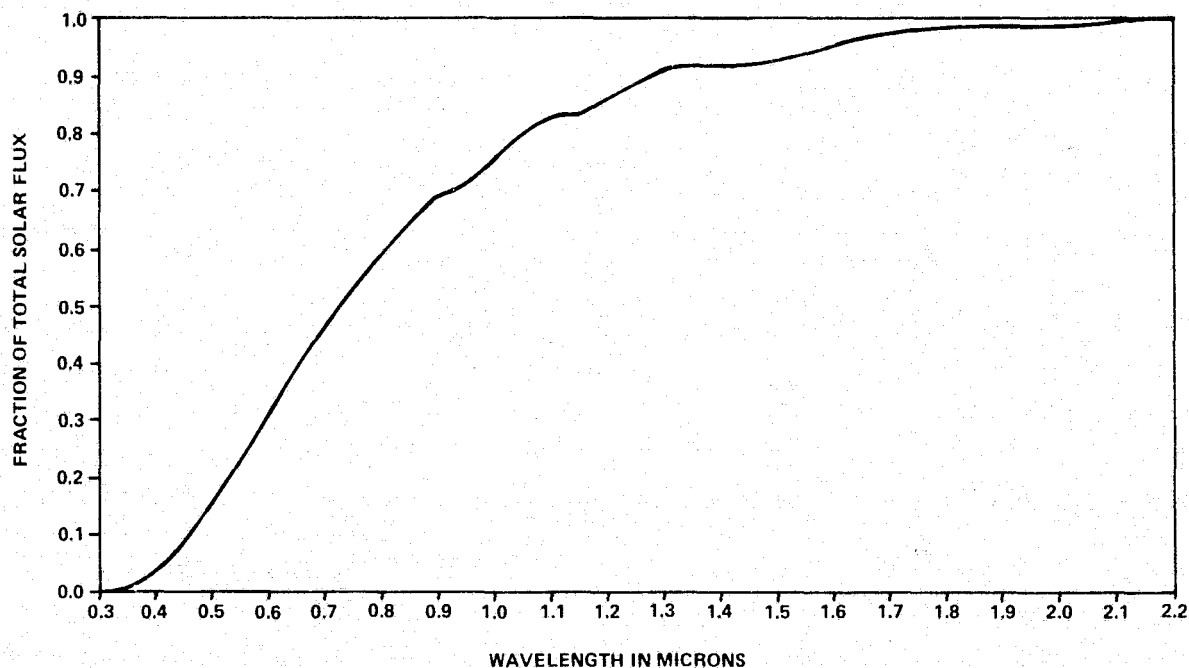
Figure 4. Energy spectrum of solar radiation.

TABLE 2. SOLAR AND LENS SPECTRAL PARAMETERS

| Wavelength Increment $(\Delta\lambda)_j$ (μ)	Center Wavelength λ_j (μ)	Weighting Factors ω_j	Acrylic Index of Refraction[6] n_j	Acrylic Bulk Transmittance Factor $(T_a)_j$
0.295-0.43	0.400	5.42×10^{-2}	1.5100	1
0.43-0.47	0.452	5.34×10^{-2}	1.5008	1
0.47-0.51	0.490	6.47×10^{-2}	1.4975	1
0.51-0.56	0.535	8.06×10^{-2}	1.4945	1
0.56-0.62	0.590	9.47×10^{-2}	1.4916	1
0.62-0.69	0.654	10.89×10^{-2}	1.4892	1
0.69-0.77	0.727	10.02×10^{-2}	1.4871	1
0.77-0.86	0.814	10.31×10^{-2}	1.4852	1
0.86-1.01	0.944	10.56×10^{-2}	1.4833	1
1.01-1.21	1.076	10.16×10^{-2}	1.4822 (Extrapolated)	0.971
1.21-2.2	1.526	13.30×10^{-2}	1.4810 (Estimated)	0.684

13
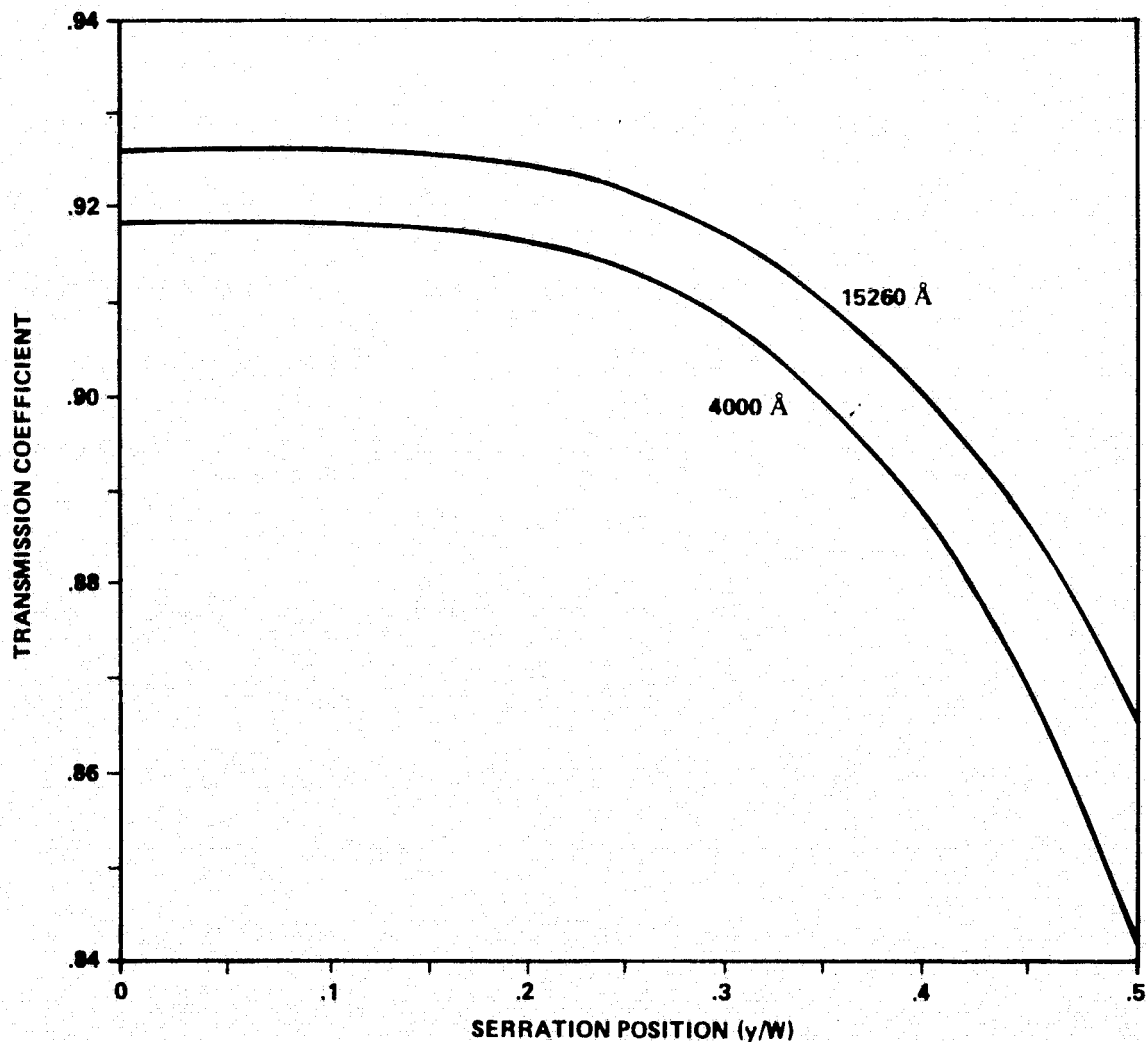
Figure 5. Transmittance versus serration position and wavelength with reflection losses only.

of the solar spectrum and bound approximately 90 percent of the total solar flux. Due to the increasing groove angle and consequently increasing angle of incidence, the transmission decreased 6 to 8 percent with increasing serration distance from the length axis of the lens. However, the average reflection losses were approximately 10 and 9 percent at 4000 Å and 15 260 Å respectively, indicating an insignificant wavelength effect. The total transmittance losses (absorption included) were calculated using equation (16) and are presented in Figure 6(a). An average lens transmittance of 87 percent resulted and indicated approximately 4 and 9 percent in absorption and reflection losses, respectively.
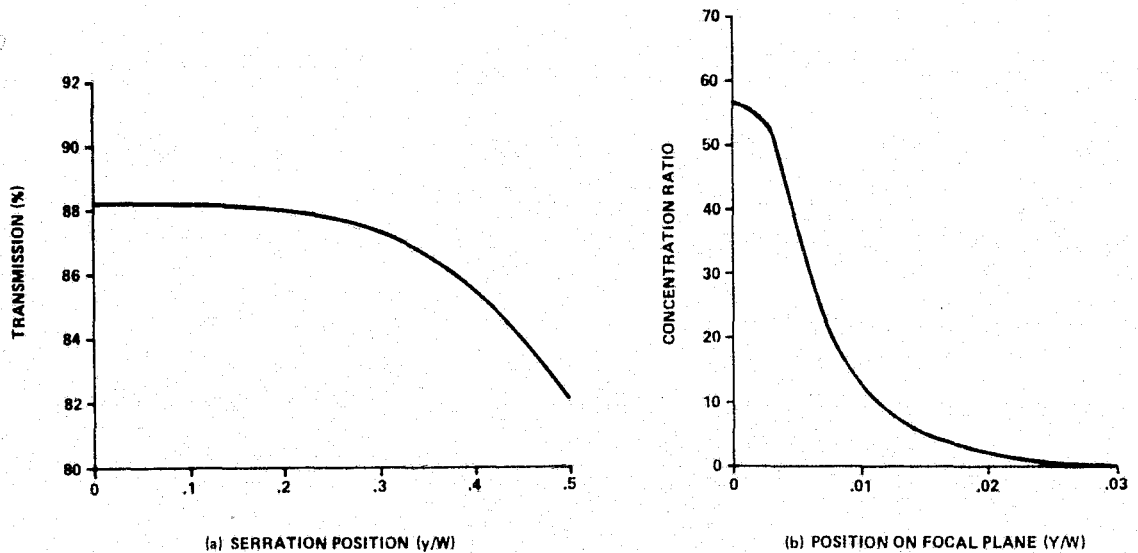
Figure 6. Lens transmission and focal plane intensity profile.

B. Focal Plane Concentration

The maximum spread of sunlight refracted to the focal plane by individual serrations was studied using equations (25) through (31). The extreme intercept positions Y_r and Y_ℓ versus serration position for wavelengths of 4000 Å, 5893 Å, and 15 260 Å are presented in Figure 7 and illustrate the effects of wavelength on refracted beams. At 4000 Å (near UV), the index of refraction is high and the intercepts become negative for serrations located greater than approximately 0.15 W from the axis. For the IR wavelength (15 260 Å) both intercepts become positive for all serration positions exceeding 0.25 W, illustrating that the refraction is less than desired. As expected, near the design wavelength of 5893 Å, all serrations contribute to the focal line intensity.

The concentration ratio as a function of position in the lens focal plane has been determined through equation (23). The procedure involved calculating the weighted intensity profile $I_j(Y)$ for each of 11 wavelength intervals (Table 2), then summing the contributions at position Y for each wavelength.[1] Figure 8 illustrates the weighted focal plane profiles for four wavelength intervals. The total concentration profile is presented in Figure 6(b) and exhibits a rather

---

1. Eleven divisions of the solar spectrum were used for most computations. Insignificant smoothing of the data resulted with 22 divisions.
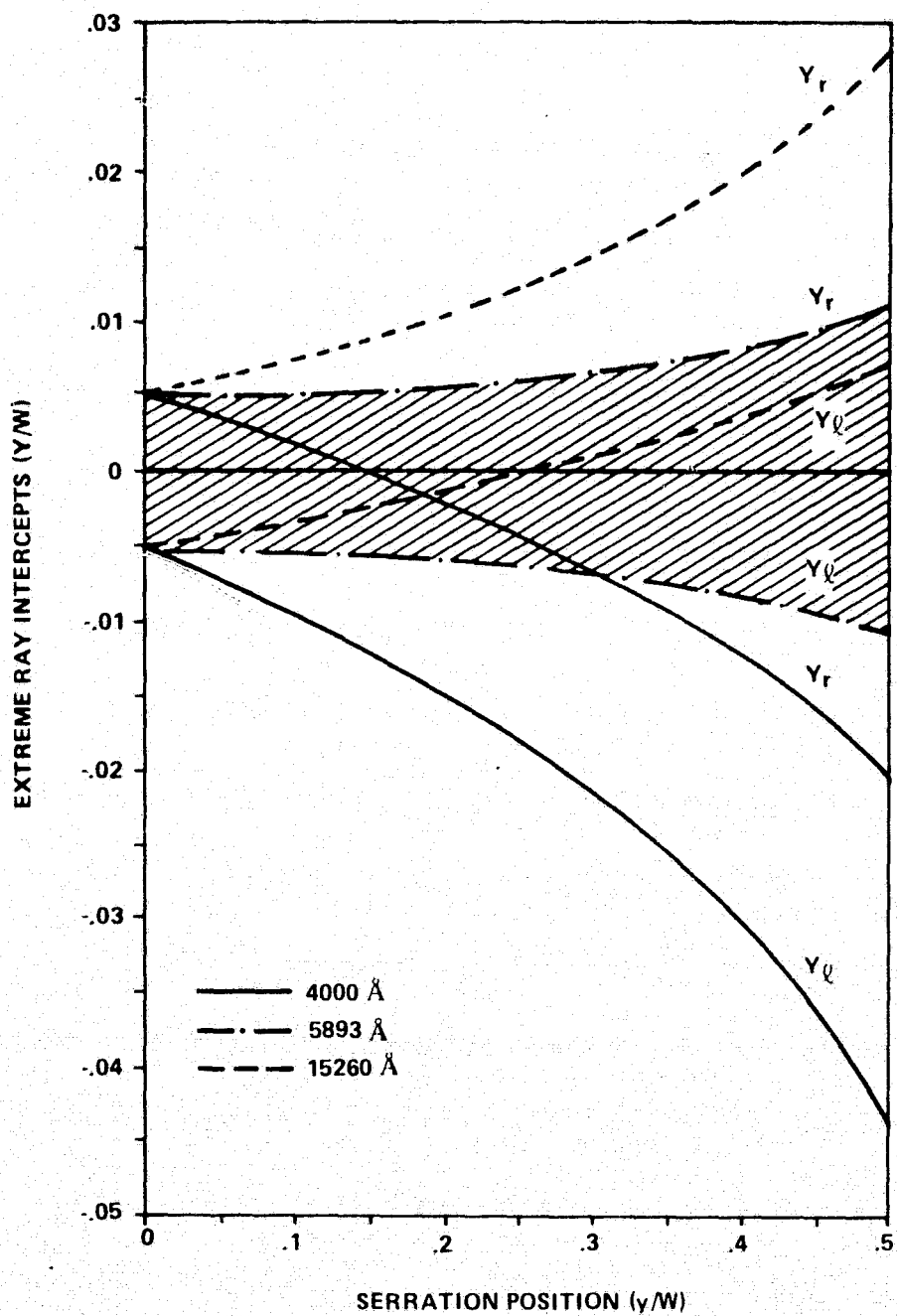
Figure 7. Extreme ray intercepts on focal plane for various wavelengths.

16

CONCENTRATION RATIO

POSITION ON FOCAL PLANE (Y/W)
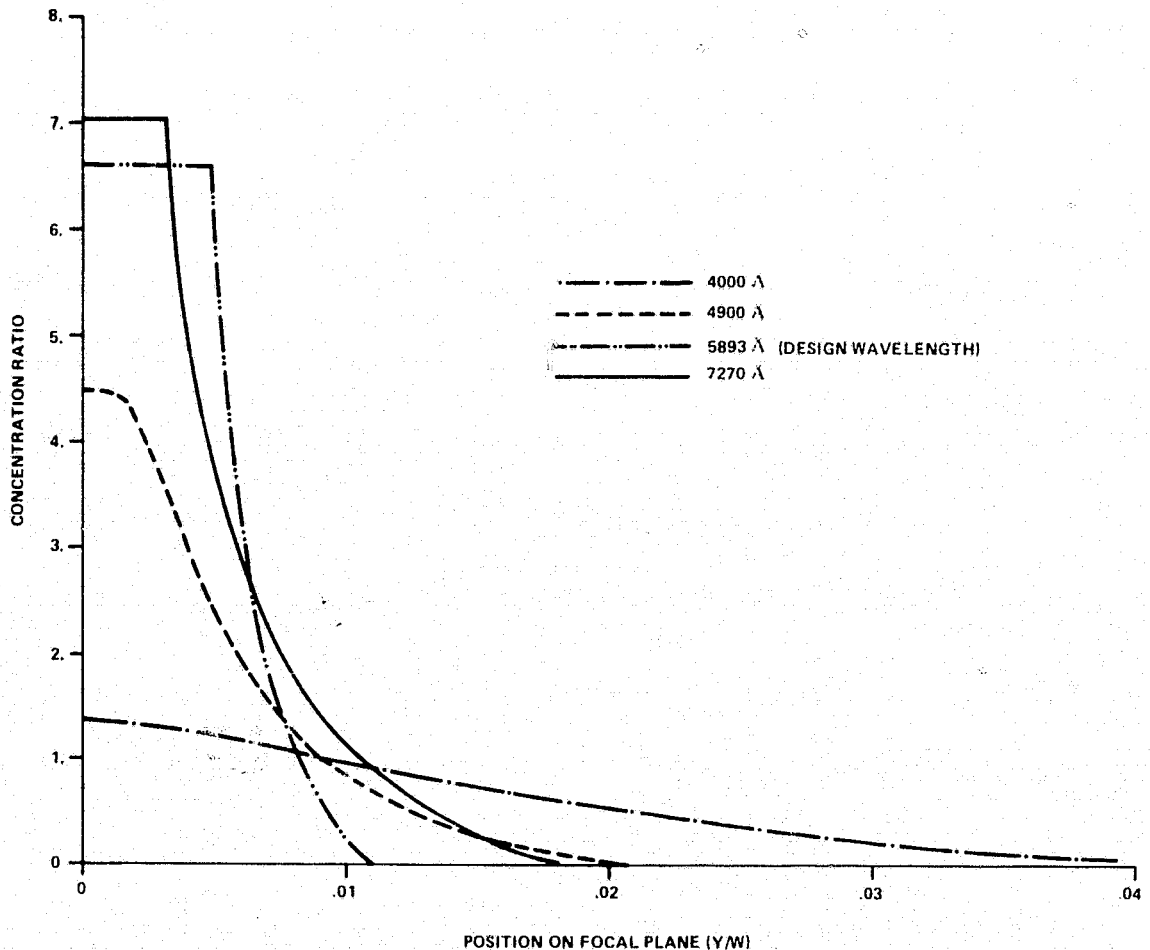
4000 Å
4900 Å
5893 Å (DESIGN WAVELENGTH)
7270 Å

Figure 8. Weighted intensity profiles for selected wavelengths.

sharp center peak with a maximum concentration of 57 and a long low-amplitude "tail". Figure 8 shows that this "tail off" results from the refraction of sunlight wavelengths far removed from the design wavelength. A quantitative measure of the energy spread is the target width necessary to intercept a given percentage of the transmitted sunlight. For example, a 90 percent target intercept width of 0.025 W was determined for the computed profile.

The influences of various analytical modeling assumptions on the computed concentration characteristics are illustrated in Figure 9. Assuming an average constant wavelength (5893 Å) resulted in a flattened profile at the peak and a narrowed width at the base. The computed maximum concentration decreased from 75 to 61 when solar dispersion was considered; whereas, the 90 percent target width increased from 0.7 to 1.4 cm. The transmittance remained constant at 91 percent. The inclusion of absorption lowered the peak
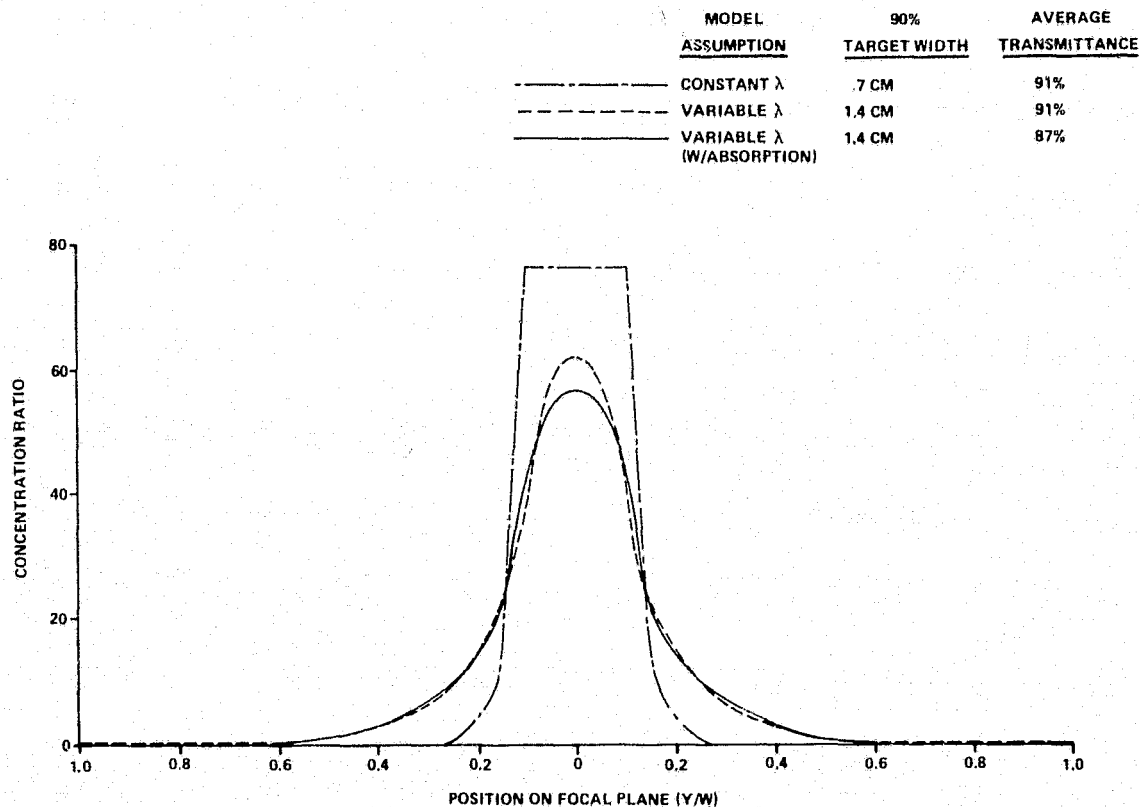
17

Figure 9. Effects of theoretical model assumptions on concentration profiles.

concentration to 57 and the average transmittance to 87 percent without altering the target width. The most significant conclusion, then, is that solar wavelength distribution has a marked effect on the calculated concentration profile, especially the width.

Also, it was concluded that design wavelength choice influences the lens solar concentration properties. A brief study indicated the peak concentration ratio is maximum at a design wavelength of 7200 Å, which represents the midpoint of the solar energy spectrum. Because the total transmittance remains practically constant, an increase in peak concentration ratio was accompanied by a narrowing of the intensity profile at the focal plane. The subsequent 15 percent reduction in 90 percent target width over that required with a 5893 Å design wavelength indicates that design wavelength optimization should be considered in future lens selections.

C. Defocusing

Concentration profiles for selected intercept planes above and below the focal plane are presented in Figure 10. In a highly defocused position, the concentrated sunlight is spread over a considerably larger region than at positions near the focal plane. To quantitatively compare the defocused profiles, the fraction of transmitted flux intercepted by a target placed in the chosen plane was determined as a function of target width for each intensity profile with negative defocusing. Figure 11 illustrates the results and indicates, for example, that the target width corresponding to a 0.9 intercept fraction at the focal plane would have an intercept fraction of 0.54 with -5 percent defocusing.

For a given intercept fraction, the target should be placed beneath the lens in a plane where the corresponding target width is minimized. Figure 12 presents 90 percent target width as a function of the defocusing percentage and indicates a minimum target at approximately the 1 percent defocused position. Further, the intensity profiles for 0, 1, and 2 percent defocusing are not strikingly different in shape (Figs. 6 and 10). The small increases in target width arise from decreases in the maximum concentration ratio, with a redistribution of the flux along the "shoulders" of the curves. The shallow nature of the minimum in the curve in Figure 12 reflects this behavior.
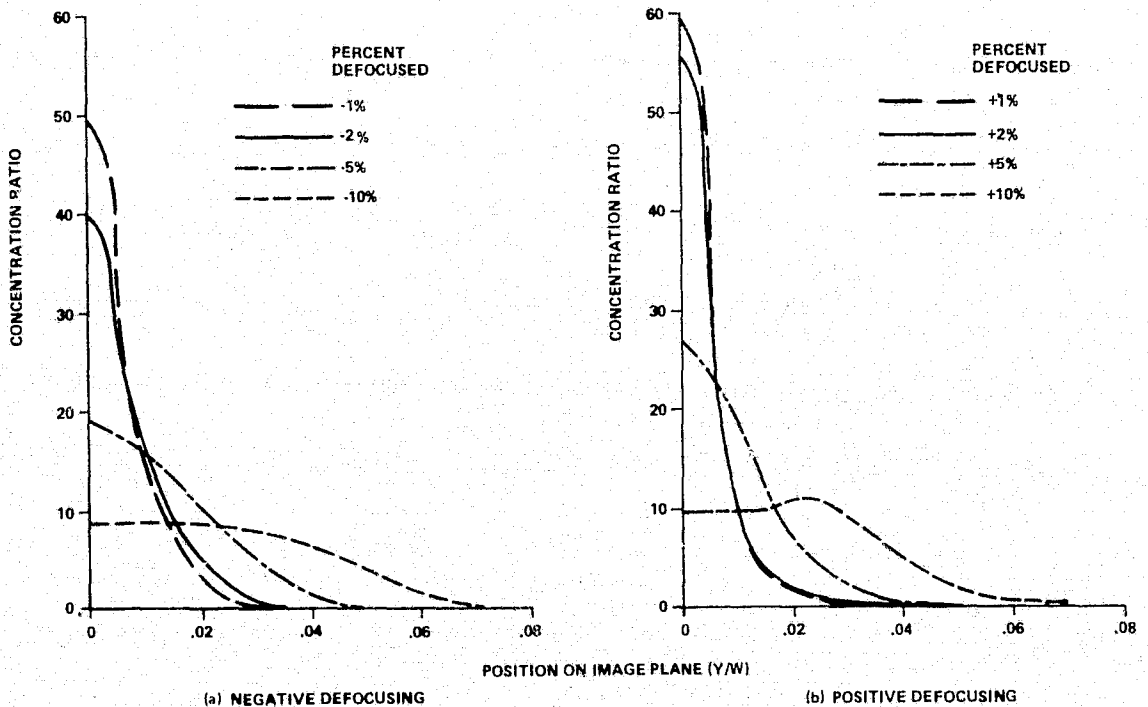

(a) NEGATIVE DEFOCUSING   (b) POSITIVE DEFOCUSING

Figure 10. Defocused intensity profiles above (-) and below (+) the focal plane.
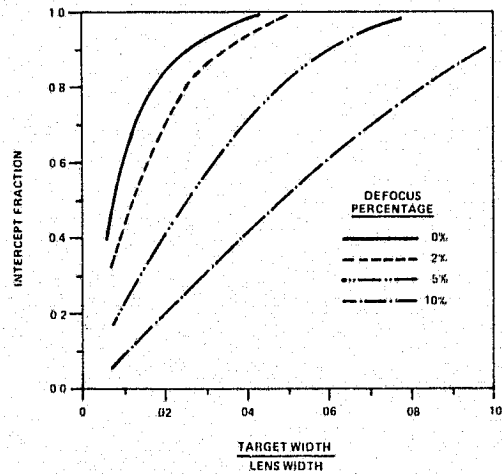
19

Figure 11.   Intercept fraction versus target width with negative focusing.
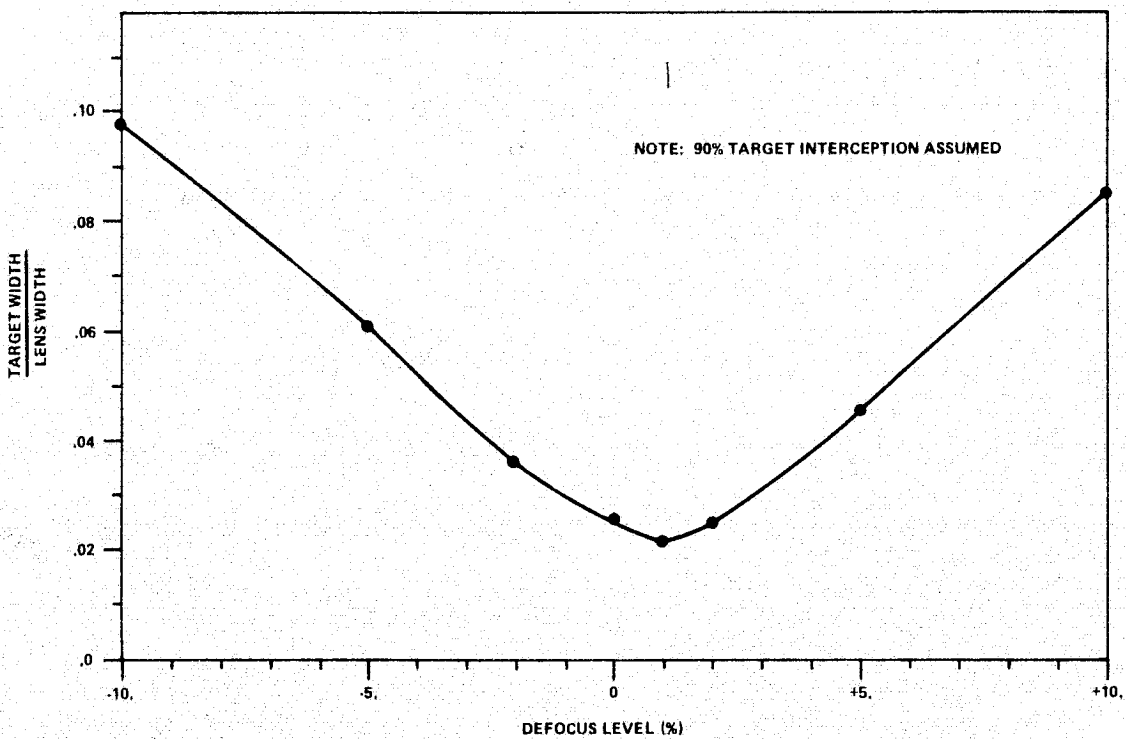

Figure 12.   Target width variation with defocusing.

20

IV. EXPERIMENT HARDWARE AND PROCEDURE

A. Lens and Overall Test Setup

The experimental 56 cm lens was formed from panels, each 28 by 38 cm produced in an exploratory, low cost fashion. Therefore, the lens quality does not represent the best now obtainable, but was adequate to examine significant performance trends. Specific deficiencies include: (1) small dimples (1 in. diameter or less) on smooth surface, (2) tool chatter marks on groove walls, and (3) some panel warpage. Modified fabrication techniques have subsequently resulted in improved lens panels. Eight panels were used to assemble a 56 by 152 cm lens (Fig. 13) which was utilized to qualitatively demonstrate the concept of developing a large scale lens from multiple panels within existing manufacturing capabilities.

Quantitative data were obtained by testing a pair of the lens panels using the overall setup depicted in Figures 14 and 15. Two panels, which formed a lens 56 by 38 cm, were secured in a wooden frame. The solar sensor was mounted to enable its translation across various planes at and near the theoretical focal plane, 56 cm from the lens. The Sun tracking heliostat provided a

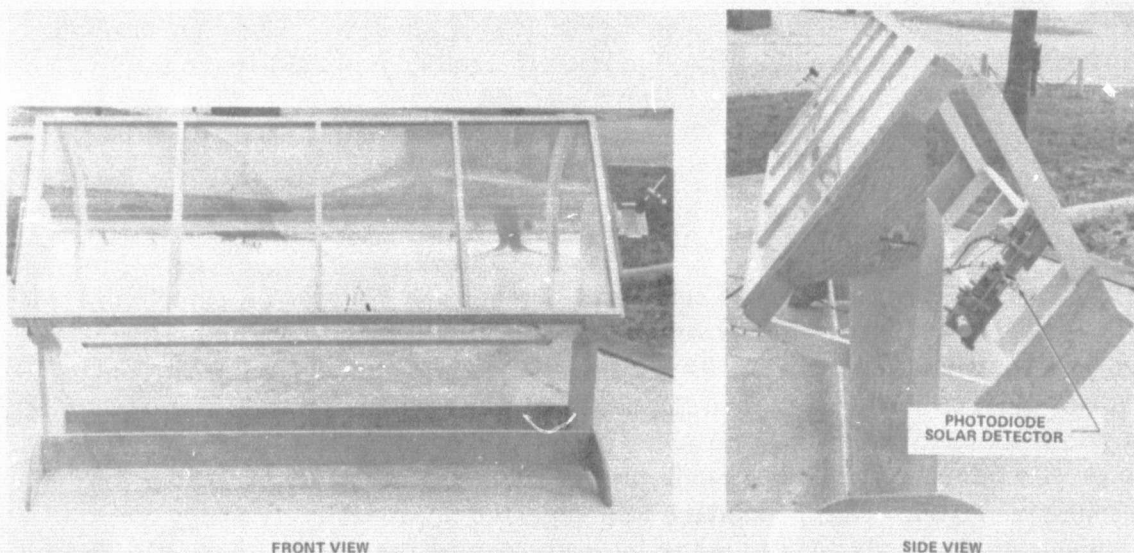FRONT VIEW   SIDE VIEW

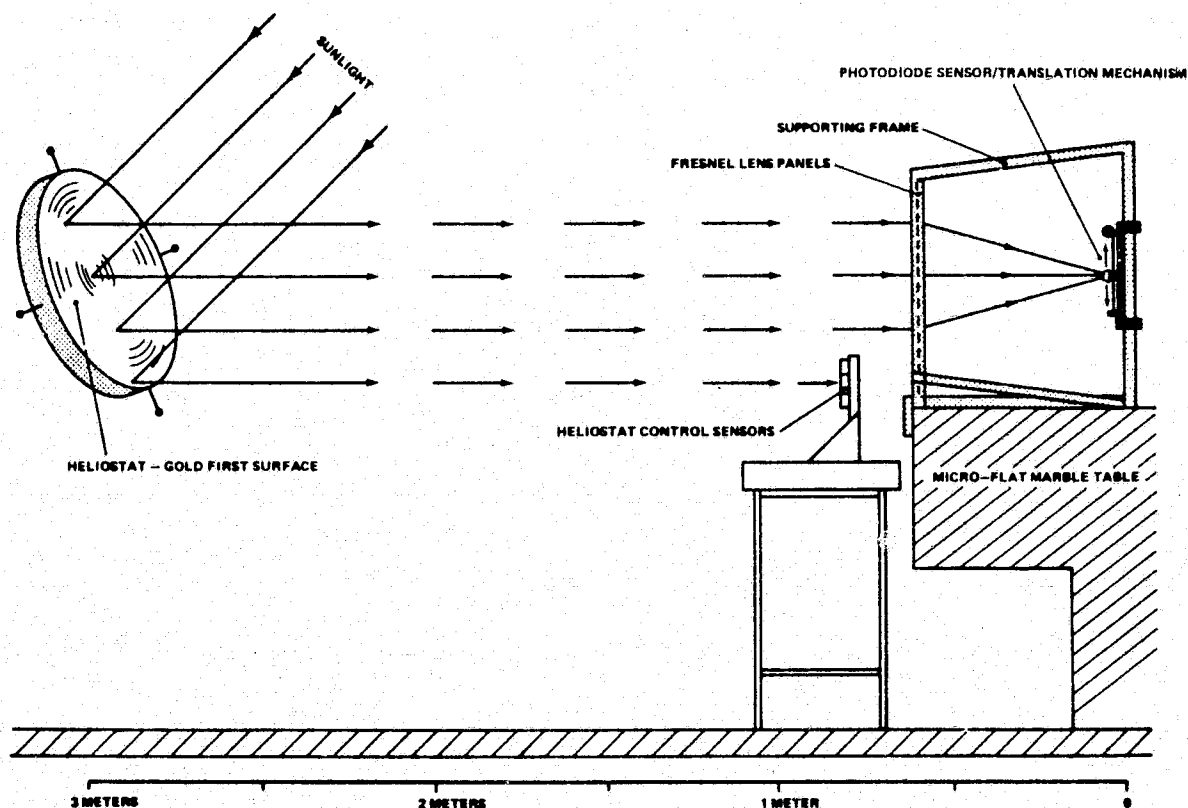Figure 13. Assembled Fresnel lens, 56 by 152 cm.

Figure 14. Fresnel lens test setup.

nonmoving Sun relative to the fixed lens and is a gold first-surface mirror, 118 cm in diameter. The Sun rays reflected to the lens were controlled to within 4 arc s of the perpendicular by the heliostat control sensors. Lens Sun tracking deviations were simulated by tilting the lens at fixed angles relative to the reflected rays.

B. Test Procedure

The tests were conducted between 10:00 am and 2:00 pm on cloudless, low haze days to minimize variations in incident flux intensity. The heliostat beam was positioned to fully illuminate the total lens width and heliostat control sensors. During each test period the baseline flux incident on the front of the lens was measured with the same solar sensor used behind the lens. A reference profile corresponding to a perfectly positioned lens (no Sun tracking error) was then measured. This procedure was repeated approximately every 30 min to compensate for variations in solar intensity during the 4 h test period. The reference plane profile was then used as a basis for establishing deviations in
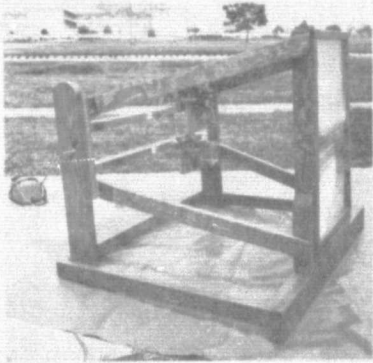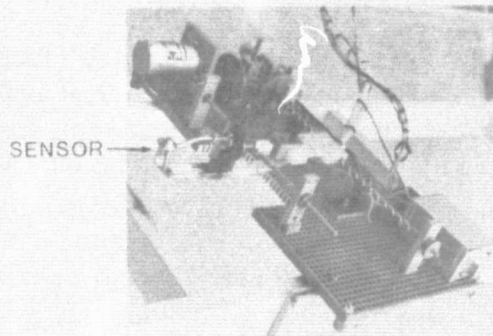
MOUNTED LENS PANELS
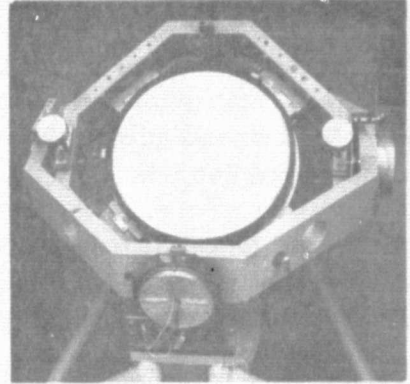
HELIOSTAT

SENSOR→

PHOTODIODE TRANSLATION MECHANISM

Figure 15. Photographs of test hardware.

image width, concentration ratio, and lens transmittance efficiency for the following test parameters: (1) transverse Sun lens orientation errors, (2) longitudinal orientation errors, and (3) defocusing.

Orientation error effects were measured by rotating the lens support frame on the optically flat marble table. Transverse tracking errors were simulated by tilting the lens support frame forward and backward about the frame base. Longitudinal (axial) tracking deviations were simulated by rotating the lens frame about an axis perpendicular to the marble table surface.

During the course of testing, the sensor response was noted to be a function of incident ray angle. Thus, the focused energy was not fully indicated by the sensor because it was translated across a focal plane in a fixed orientation, i.e., it was approximately 15 percent low. Therefore, the baseline

concentration profile and lens transmittance were established by orienting the sensor axis approximately parallel to the focused rays from lens sections as the sensor was moved across the image plane. To preclude excessive test periods, the measured Sun tracking and defocusing data were obtained without adjusting the sensor axis, i.e., the sensor axis was maintained vertical to the focal plane of interest. Therefore, the profiles measured to evaluate "off-baseline" conditions do not represent the total transmitted energy, but are sufficiently accurate to define relative profile shapes. It is important that the effects of this test technique be considered in the utilization of experimental data presented herein.

C. Instrumentation

The solar sensor consists of a photodiode mounted (Fig. 15) in a water cooled fixture to maintain acceptable temperatures. Additionally, the fixture surface is conically shaped and chrome plated to reduce the absorbed thermal radiation. The mounting fixture is attached to a mechanism which allows the photodiode to scan an adjustable distance across the selected image plane. Movable limit switches are installed which control the sensor scan distance. The sensor distance from the lens can be adjusted ±1.27 cm from a given plane without moving the entire mechanism. The photodiode signal is sent through a current to voltage converter and is then recorded by a Moseley 7100B strip chart unit. Calibration scales on the Moseley unit were selected to utilize the full scale of the chart paper to record the concentration profiles, thereby, enhancing the accuracy of profile comparisons and analyses.

The sensing element is basically a silicon phototransistor (Spectronics Inc. Sensor SD-3443-3) which is modified and used as a photodiode. Details on the sensor modifications, electrical circuit, and response properties are presented in Appendix A. The spectral response of the SD-3443-3 peaks at 8500 Å and has a 20 percent relative response at 4000 Å and 10 700 Å. A constant response across the solar spectrum was desired, but it was reasoned the expression of energy transmitted through the lens in terms of concentration ratio would eliminate sensor errors that would otherwise occur in measuring absolute magnitudes. However, a subsequent concern was that the lens would alter the solar energy wavelength distribution causing erroneous data. Thus, the utilization of a thermopile sensor (Sensor, Inc. Type L22-CF-3), which has a constant spectral response, was attempted. However, the sensor was unsuitable because of slow thermal response characteristics. Also, at high concentration levels erroneous readings occurred, apparently due to heat leakage between the sensing element and reference junction. Finally, the thermopile sensor was

used to establish accuracy of the photodiode by comparing the two instruments at low concentration levels. Details on the photodiode accuracy verification procedure are presented in Appendix B.

As mentioned previously, the photodiode response variation with incident angle caused low energy readings when the instrument was translated across the concentration profile in a fixed orientation. The viewing angle/response characteristics have been improved for subsequent testing. Therefore, the instrument previously described and in Appendix A is applicable only to the experimentation described herein.

V. EXPERIMENTAL RESULTS

A. Baseline Profile

The evaluation of parameters affecting lens performance required a baseline solar concentration profile be established as a reference, preferably at the focal point. The focal point is defined as that position at which the design wavelength rays intersect beneath the lens. Thus, the actual focal length of a lens can best be located using a laser beam with the design wavelength. However, with the Sun as the source, a different approach had to be devised. Concentration profiles at various positions near the theoretical focal length of 56 cm were measured. As discussed in a subsequent section on defocusing, the maximum concentration ratio and minimum target interception width did not occur simultaneously, that is, at the same focal distance from the lens; thus, a baseline position that represented a compromise between maximum concentration and minimum target width had to be chosen.

The baseline profile measurement position selected was 56.44 cm from the lens, and the resulting profile is compared with that computed in Figure 16. A peak concentration ratio of 47 and a 90 percent target width of 3.6 cm were measured. The calculated peak concentration and target width were 57 and 1.4 cm, respectively. The reduced concentration and increased target width experimentally observed are attributed to profile spreading at the base. The measured 85 and 80 percent target widths were 2.5 and 1.9 cm, respectively, indicating the target increment was large relative to a corresponding area increment in the base region.
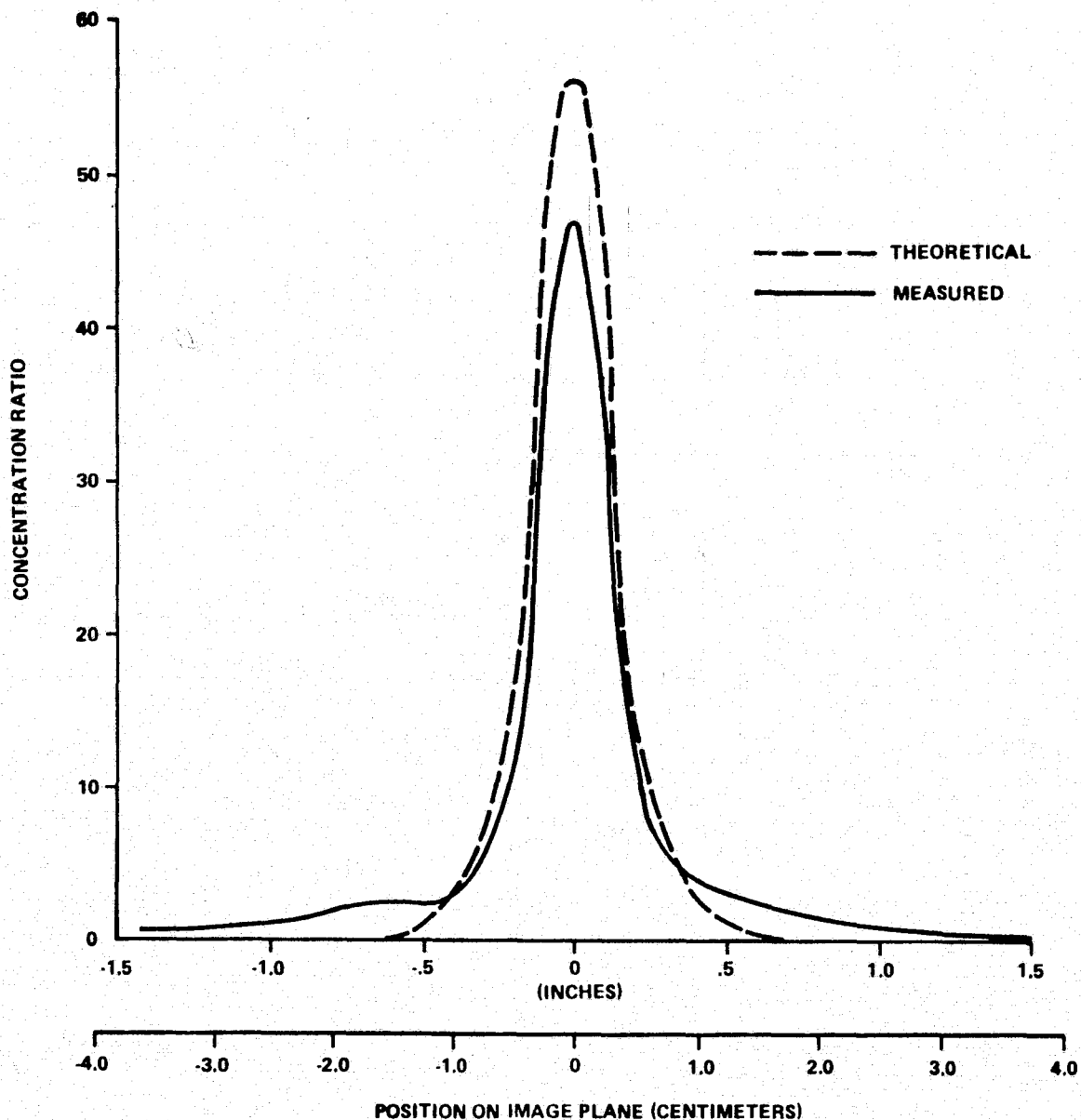
Figure 16. Analytical/measured baseline profiles.

Profile spreading at the base is attributed to the particular lens tested. As mentioned previously, the lens utilized in this test series represents the first attempt to produce a lens with high concentration. Based on preliminary component testing with subsequently produced lenses, the concentration characteristics and the corresponding target widths are much improved.[2] From a total transmittance standpoint, the 56 cm lens performed satisfactorily. An

___

2. A test program utilizing a 1.83 by 3.66 m lens is presently in progress. A peak concentration ratio of 65 and a 90 percent target width of 4 cm have been measured. The calculated peak concentration and target width were 59 and 4.3 cm, respectively.

average transmittance of 87 percent was measured and calculated. As indicated in Figure 17, the measured transmission was higher than that computed in the central region of the lens, but was lower at the outer serrations. It is speculated that the actual lens absorption was 1 to 2 percent lower than that used analytically, resulting in the "higher than computed" experimental transmittances. The low measured transmittances are attributed to slight lens warpage in the transverse direction at the outer edges.

The influences of Sun lens alignment and defocusing are presented in the following sections. Subsequent data and analyses pertain only to the 56 cm lens unless otherwise noted.
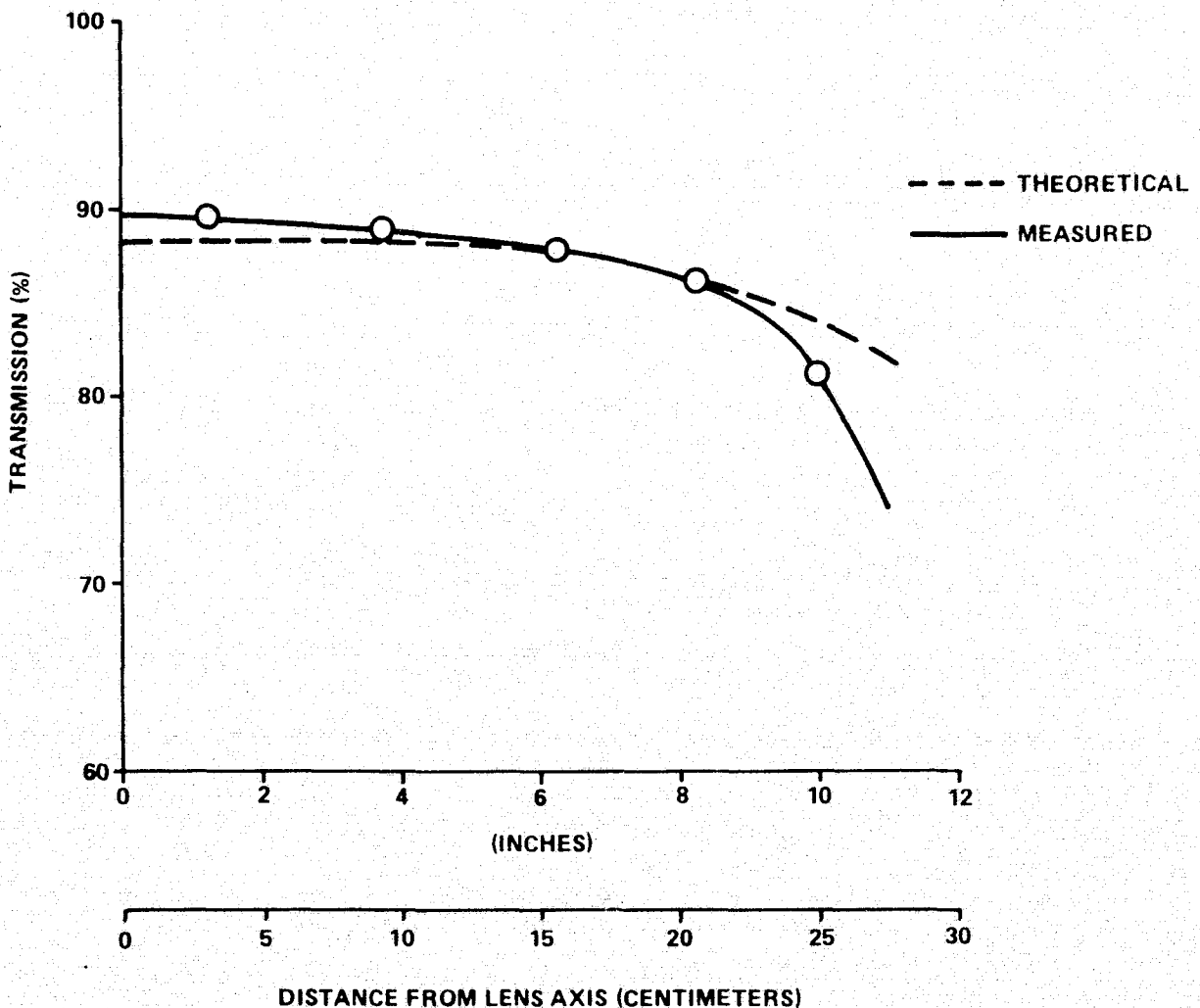

Figure 17. Analytical/experimental transmission efficiency.

B. Transverse Orientation

The measured concentration profiles corresponding to transverse orientation deviations ranging from 0.25° to 1.5° are presented in Figures 18, 19, and 20. A "no tracking error" profile is also presented in each figure for reference purposes. Visual observation of the measured data reveals that transverse deviations can modify the profiles by: (1) shifting the profile, (2) altering the profile symmetry, and (3) lowering the maximum concentration.

The lateral shifting of the concentration profile is a primary influence on the target width required for specific tracking accuracy tolerances. Assuming a 90 percent target width and referring to Figures 18, 19, and 20, a reference target width is compared with widths corresponding to the various tracking errors tested. For example, the target must be increased by 0.3 and 3.0 cm to accommodate tracking errors of ±0.25° and ±1.5°, respectively. The dependence of target width on the profile shift is more specifically illustrated in Figure 21 where the lateral shift of the peak concentration ratio and the increase in target size are presented as functions of tracking error. The measured target increase and peak concentration positions shift varied linearly with tracking error. The target increase predicted by Optical Sciences Group in Reference 2 is also presented for comparison with the measured data. The correlation is reasonable up to 1° where the predicted variation begins to exceed that measured. For design purposes, a conservative approach would be to utilize the analytical data for angles exceeding 1° until further measured data with improved lenses becomes available.

The target increase can be predicted reasonably well by adding the peak position shift for a particular orientation error to the reference target width. This general rule proved accurate for the range of orientation errors tested; however, in the case of an improved lens (one with less profile spreading) the technique may be limited to transverse tracking errors equal to, or less than 1°.

The measured transmission did not vary with transverse error. Also, although the profile symmetry was affected by transverse misalignment, the image width for an individual profile was not increased significantly. The profile base narrowing on one side apparently compensated for the broadening on the opposite side. The decrease in peak concentration ratio versus transverse error is shown in Figure 22. The concentration ratio decreased ranged from 1.0 percent at 0.50° to 17 percent at 1.5°.
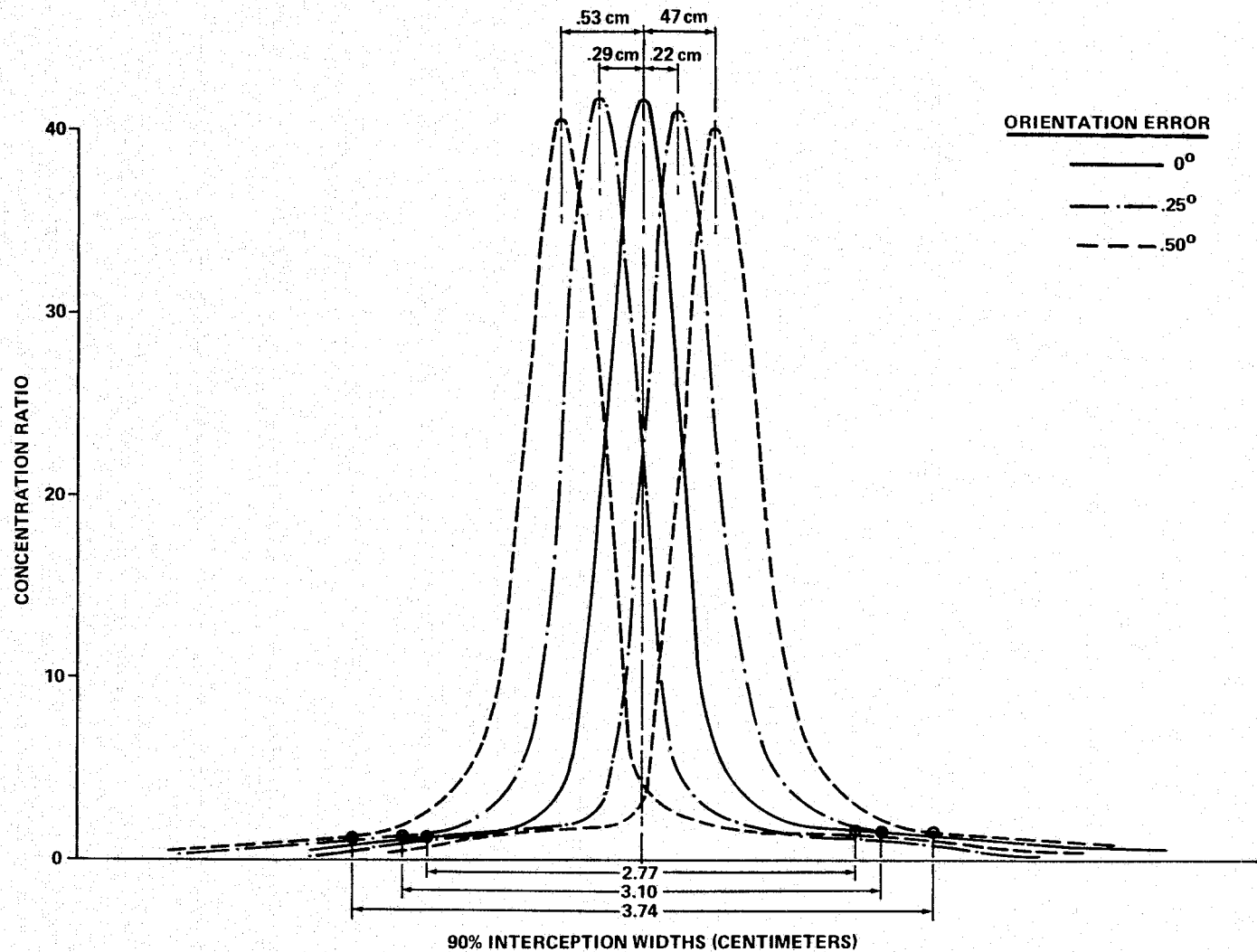
Figure 18. Measured transverse orientation effects on intensity profile.
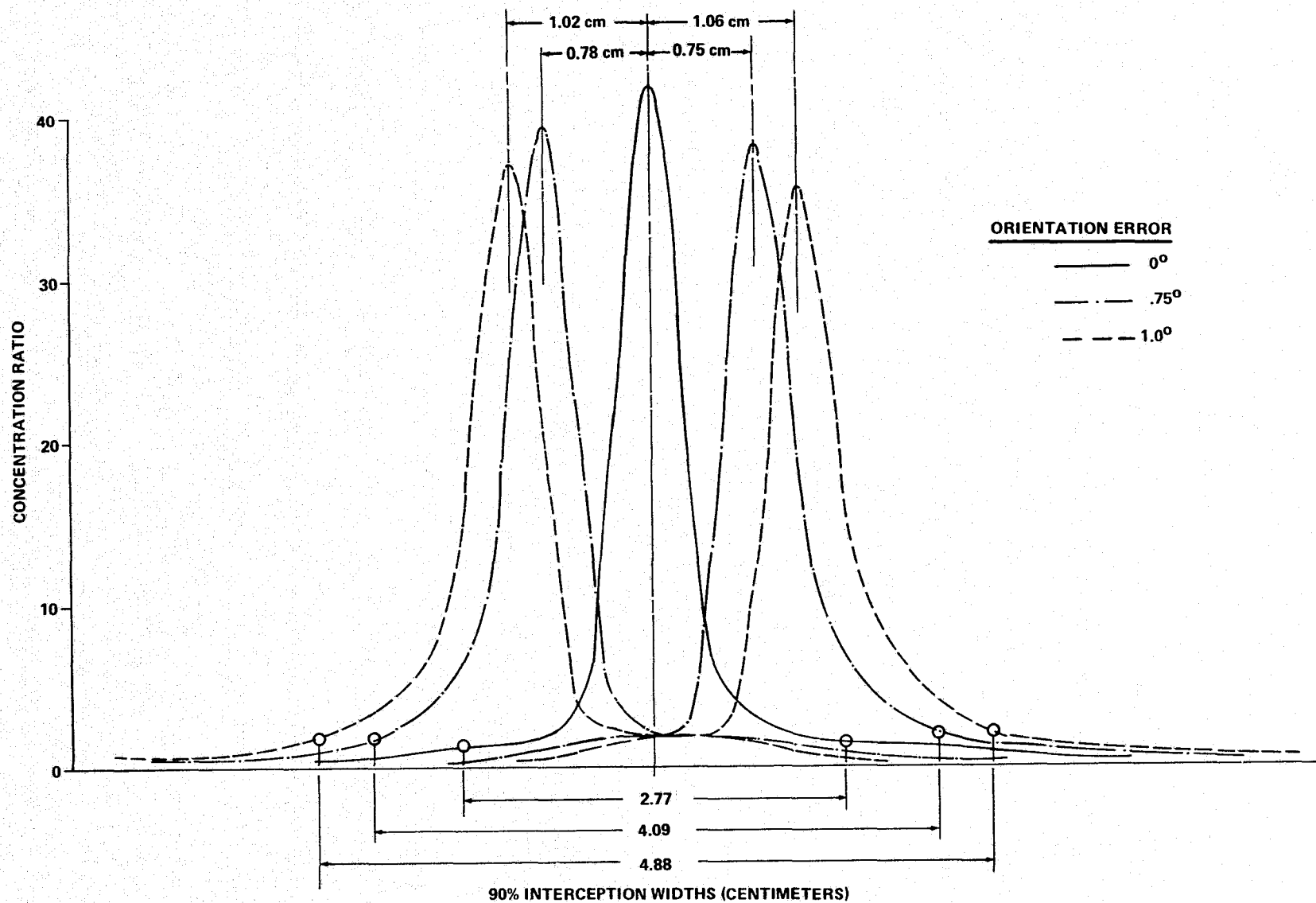
Figure 19. Measured transverse orientation effects on intensity profile.
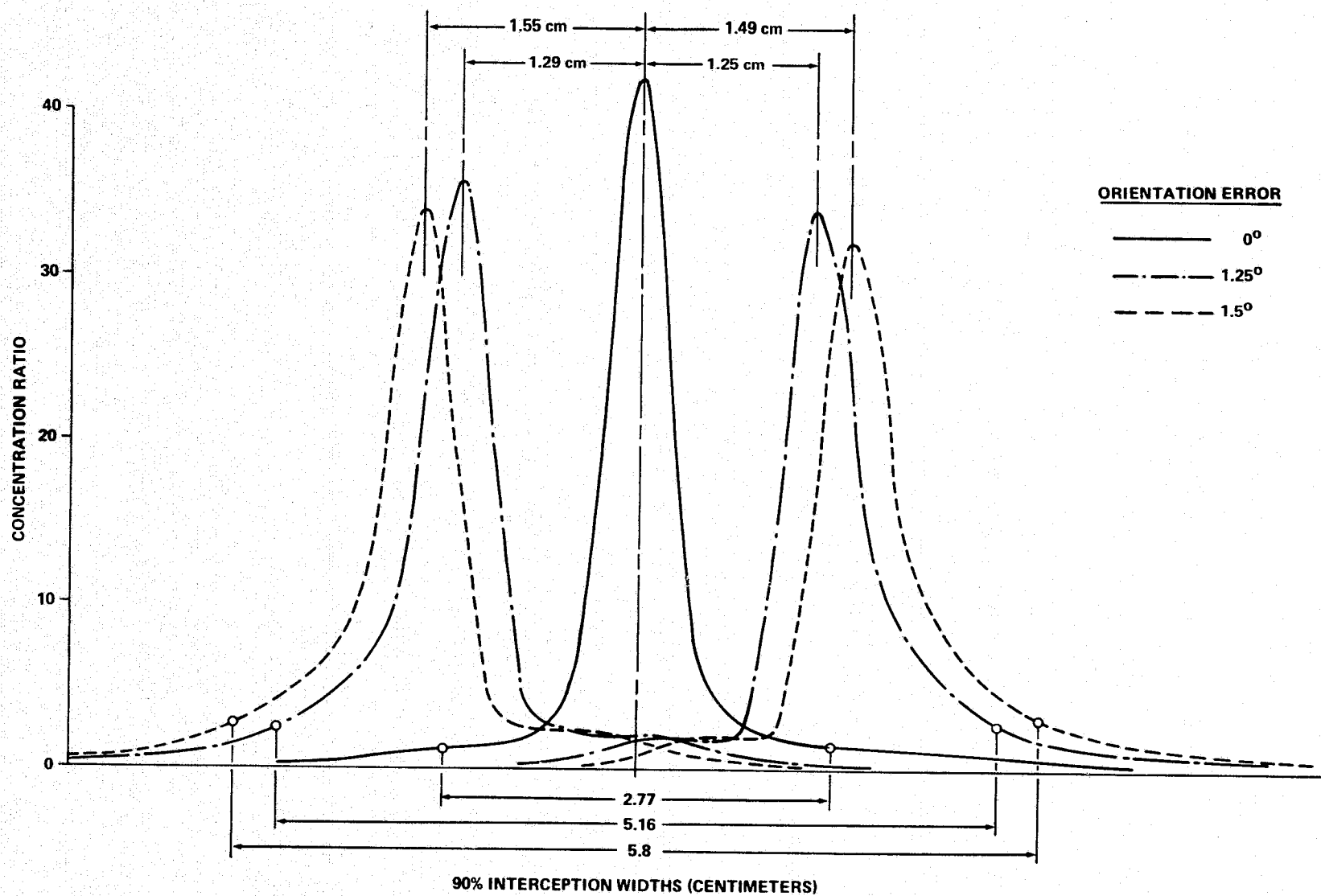
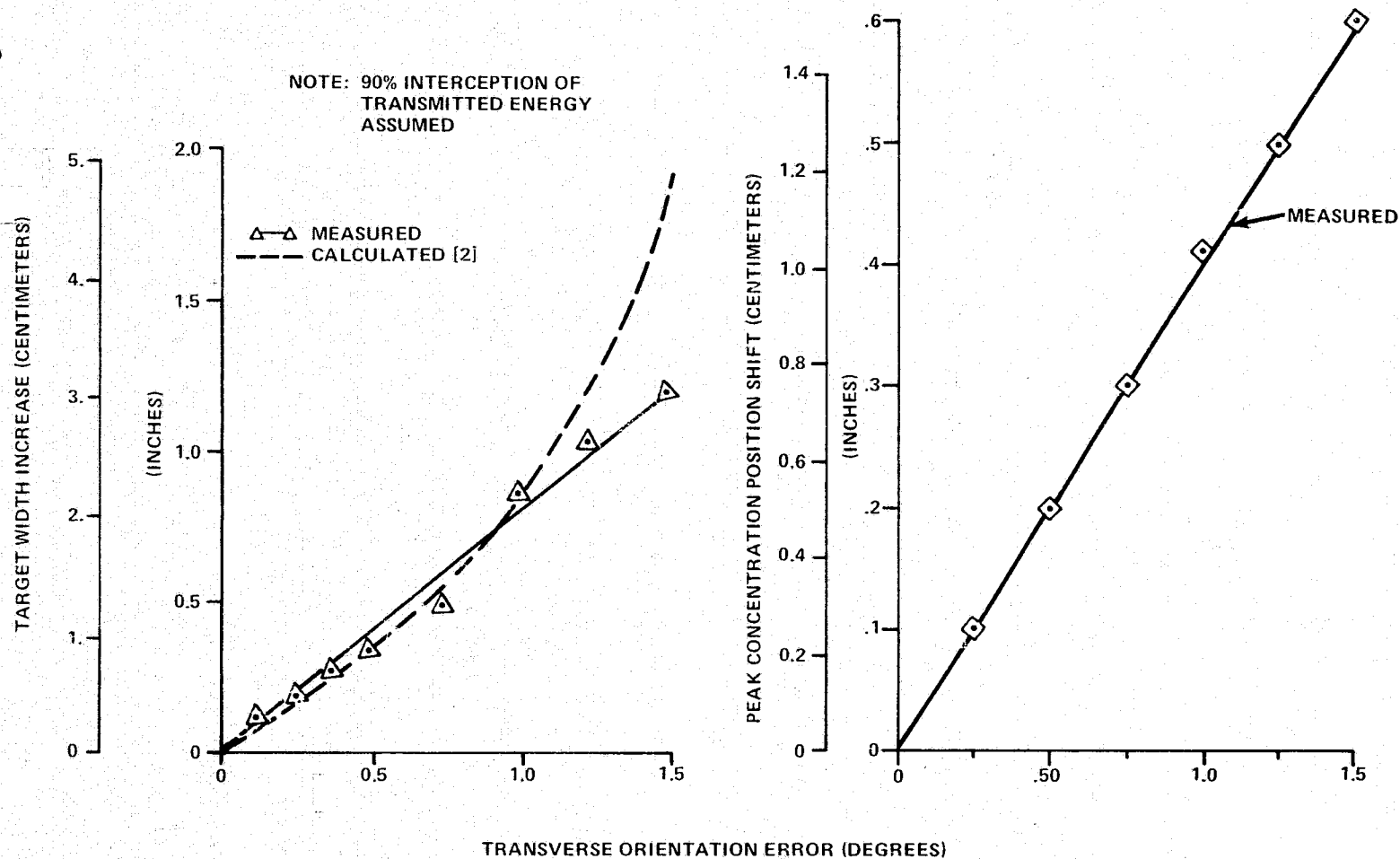Figure 26. Measured transverse orientation effects on intensity profile.

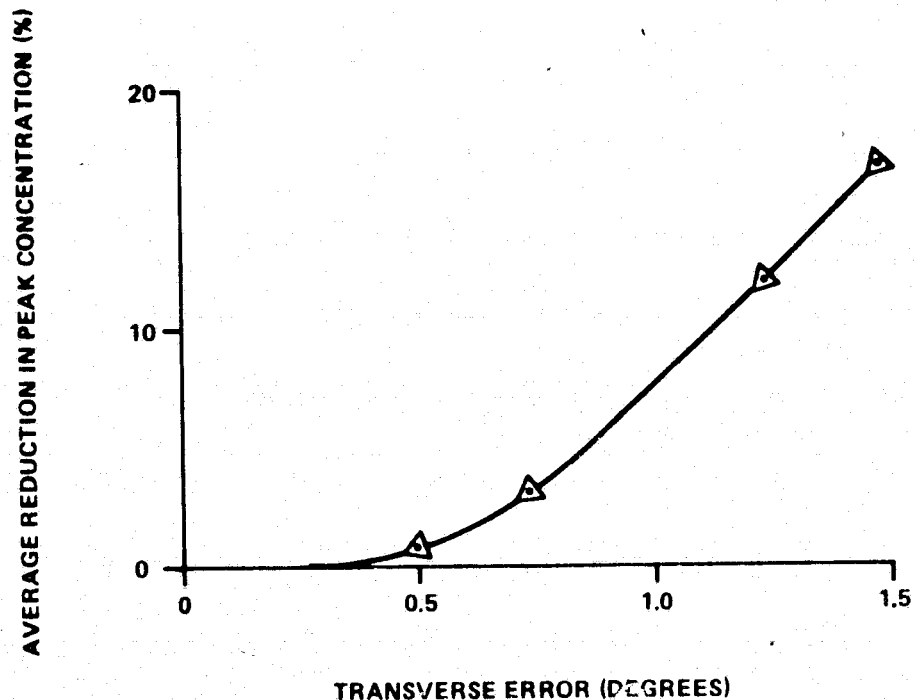Figure 21. Transverse orientation effects on target width and profile position.

Figure 22. Measured transverse orientation effects on peak concentration.

C. Longitudinal Orientation

Reference plane concentration distributions were measured with six longitudinal orientation deviations ranging from 1.5° to 9.5°. Example concentration profiles for 0°, 6.4°, 7.9°, and 9.5°, presented in Figure 23, indicate that the concentration peak decreases and the profile base broadens with increasing orientation error. However, the effects were small at low angles. A tracking error of approximately 5.0° or less had little effect on the peak concentration. Above 5.0° the peak concentration decreased rapidly with increasing angle and was reduced by 20 percent at 9.5°. At 1.6° or less, there was no increase in the 90 percent target. Above 1.6° the target width increased by 0.6 and 1.3 cm at 6.4° and 9.5°, respectively.

The lens transmission was not significantly affected. Thus, lens performance was relatively insensitive to Sun lens alignment in the longitudinal direction.
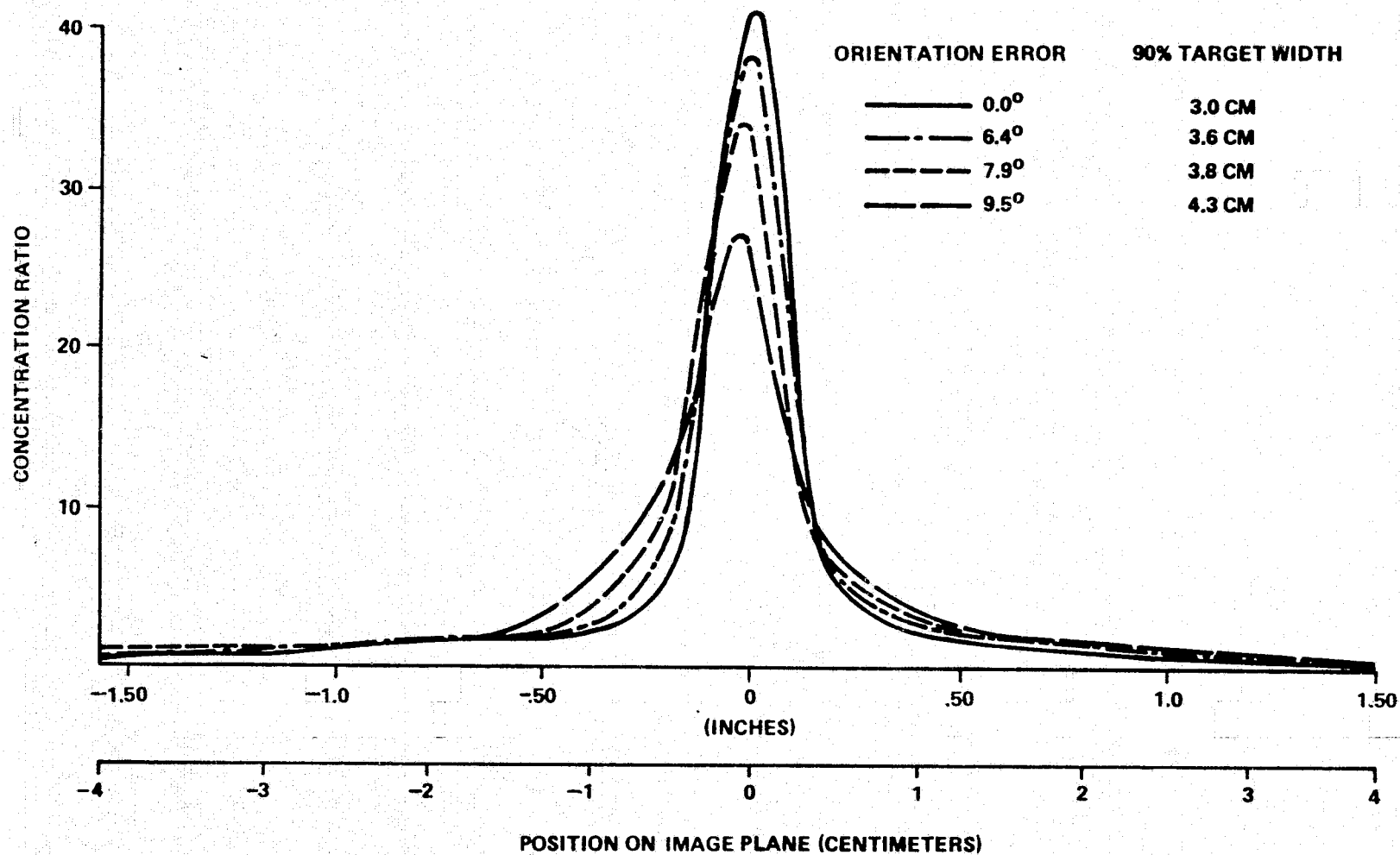
Figure 23. Measured longitudinal orientation effects on intensity profile.

D. Defocusing

The effects of moving the measurement position relative to the baseline focal length (56.44 cm) were investigated by measuring 22 profiles at positions ranging from 56.2 to 54.8 cm. The general influences of measurement position on profile shape are illustrated in Figure 24. The profiles presented include positions at 54.8, 55.3, 55.9, and 57 cm which represent defocusing percentages, relative to the baseline position, of -3, -2, -1, and 1 percent, respectively.

The results illustrate the considerations involved in establishing a baseline profile position. The focal plane obviously was not at the theoretical position of 56 cm, i.e., the profile was defocused. At the 57 cm position, the peak concentration increased to 50 and the upper portion of the profile narrowed, while its base widened. As the measurement position was moved from the baseline position toward the lens, the centerline concentration decreased, the overall profile broadened, and a "double-peak" condition occurred beginning at approximately 55.3 cm. The double-peaking is tentatively attributed to interference effects of focused rays. Measured target width as a function of distance from the lens is presented in Figure 25. No definite trends concerning the effects of defocusing on target width could be established, at least within the range of positions tested. The image spread at the base apparently "masked" the defocusing effects on target width. The average width was 2.75 cm, and variations generally were between 2 percent and -10 percent relative to the baseline width of 2.85 cm. Deviations as much as 19 and -14 percent were observed and are attributed to the acute sensitivity of the target width to the profile shape at its base. Profiles appearing to vary little in shape resulted in target widths that differed as much as 30 percent.

The measured and computed profiles for the 1 percent defocused position are shown in Figure 26. In both cases, the peak concentration increased and the overall profile narrowed relative to the focused case (i.e., the analytical/theoretical trends are comparable). Correlation of the double-peaking condition requires further study.

VI. CONCLUSIONS

1. A baseline peak concentration of 57 and a 90 percent target width of 1.4 cm were calculated for the 56 cm lens. The measured concentration and target width were 47 and 3.6 cm respectively. Spreading at the experimental profile base resulted in a lower concentration and increased image width relative to the analytical baseline.
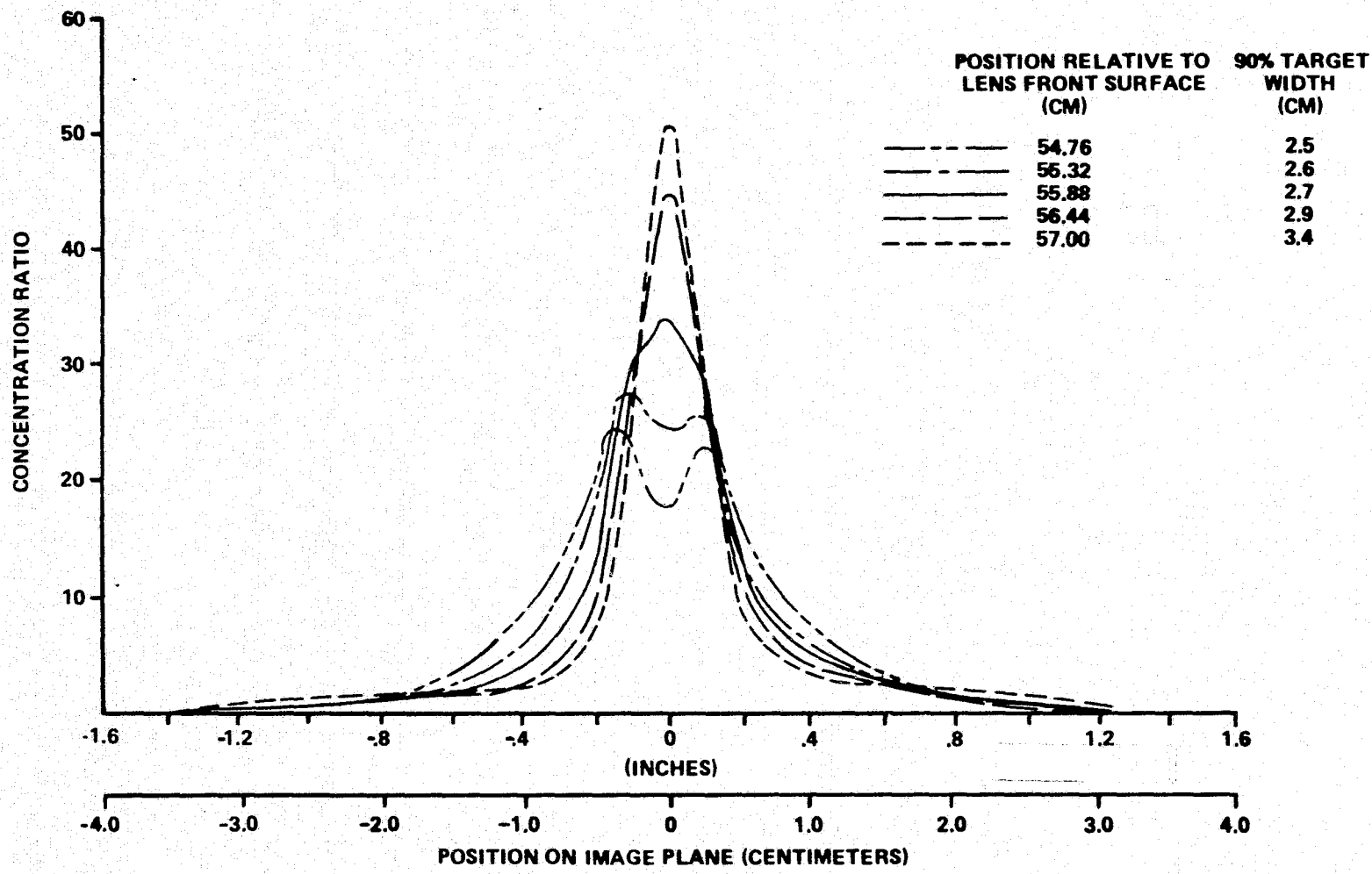
POSITION RELATIVE TO LENS FRONT SURFACE (CM)	90% TARGET WIDTH (CM)
54.76	2.5
56.32	2.6
55.88	2.7
56.44	2.9
57.00	3.4

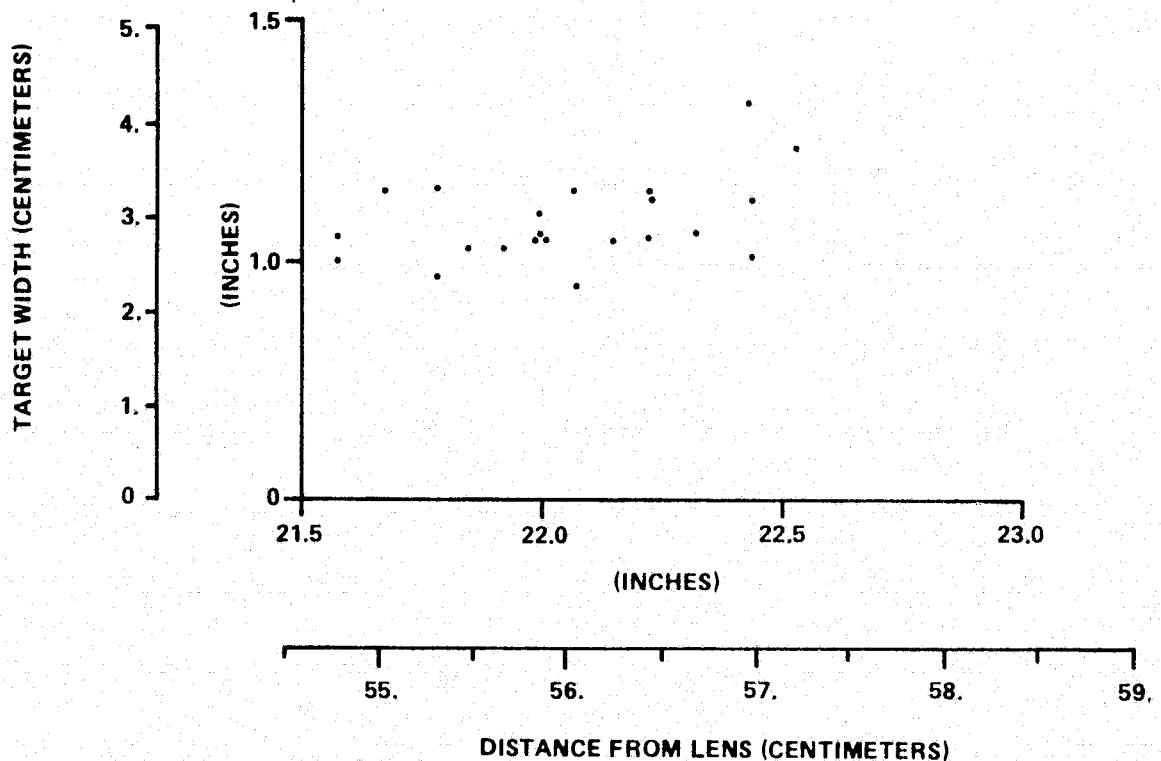Figure 24. Experimental intensity profiles with defocusing.

Figure 25. Measured target widths versus focal length.

2. Manufacturing technique modifications satisfactorily corrected the profile spreading difficulty. Preliminary testing with a second-generation lens indicates a marked reduction in profile spreading.

3. The analytical baseline profile indicated that the refraction of wavelengths far removed from the design wavelength primarily determines the image width. Concentration characteristics can be optimized by careful selection of the design wavelength.

4. Experimentally, the primary effect of small transverse Sun tracking errors (< 1°) was the lateral shift of the profile. The target width increased linearly with tracking error with an increase of 1.0 cm at 0.5°, for example. Reduction of peak concentration ratio and increased profile skewness occurred with greater misalignment.
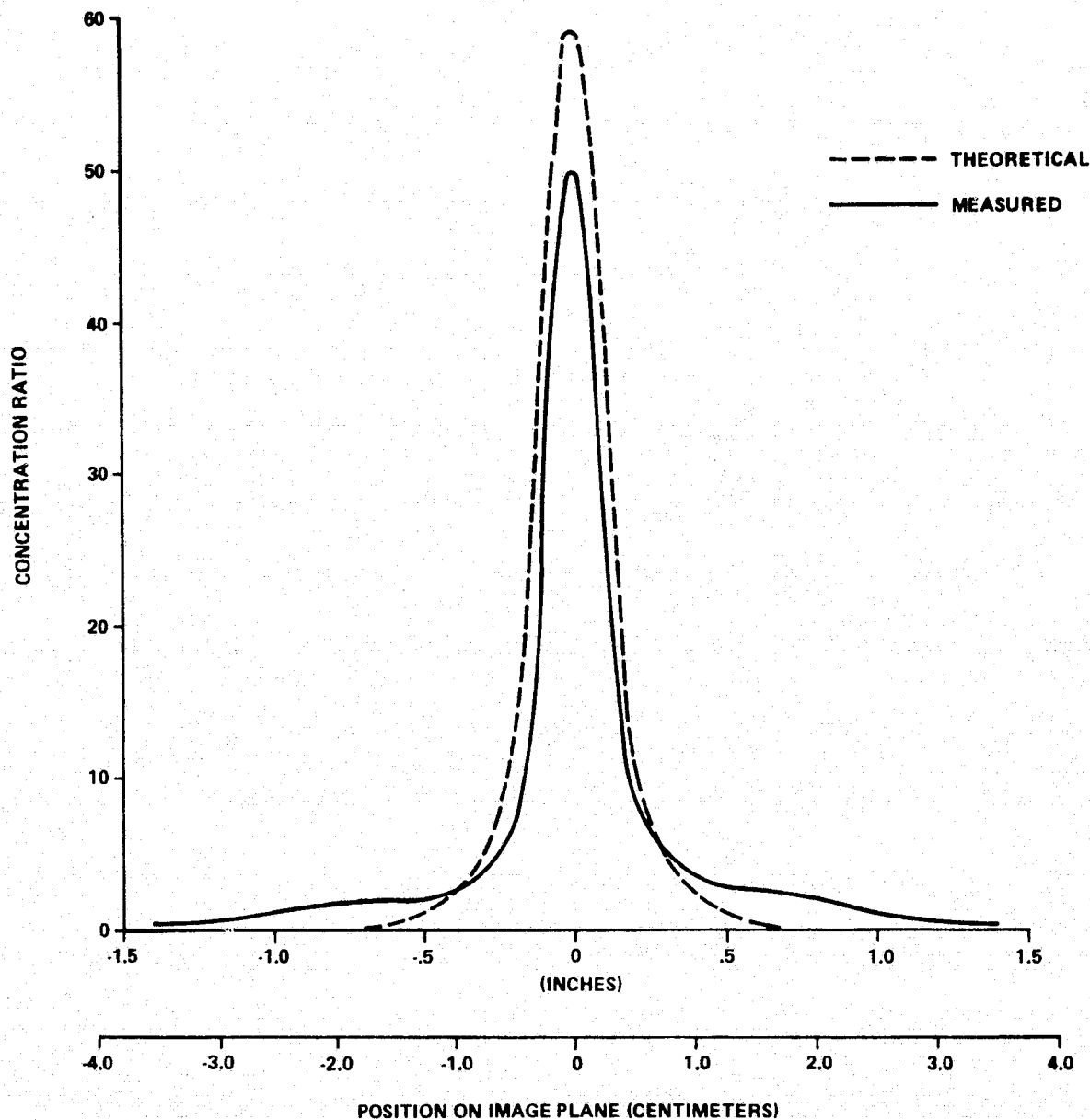
Figure 26. Analytical/experimental intensity profiles with
1 percent defocusing.

5. At deviations below 5.0°, longitudinal orientation effects on lens performance were insignificant. Above 5.0°, peak concentration decreased and target width increased rapidly; e.g., at 9.5° the peak concentration had been reduced by 20 percent and the target width increased by 1.3 cm.

6. High lens transmittance was computed (87 percent) and measured (85 percent) and was not significantly affected within the range of tracking errors evaluated. Computed reflection and absorption losses were 9 and 4 percent, respectively.

7. For the chosen lens parameters, analysis revealed a maximum peak concentration ratio (59) and a minimum target width (1.2 cm) with 1 percent defocusing (away from the lens). Experimental results indicated slight defocusing can result in more desirable profile characteristics from a thermal design standpoint, i.e., equal energy interception can occur with decreased thermal gradients. Profile spreading compromised evaluation of experimental defocusing data relative to target width.

8. The utilization of a thermopile sensor to measure the concentration ratio profiles was attempted because of its superior spectral response characteristics relative to those of a photodiode sensor. However, the thermopile proved inadequate due to its slow thermal response and heat short problems at high concentration levels. A comparison test at low concentration levels proved the photodiode sensor accurate.

9. Utilization of the heliostat to provide a nonmoving solar source proved to be a good approach. Frequent adjustments of experimental apparatus and test parameters were accomplished independent of the Sun tracking portion of the test setup. Precise control of prescribed Sun lens alignment deviations was also enabled.

APPENDIX A

SOLAR DETECTOR DESCRIPTION

An electrical schematic of the solar energy detector is shown in Figure A-1. Q1 (the SD-3443-3) is a light sensitive transistor connected and used as a photodiode. The connection takes advantage of the base current sensitivity to temperature variation being approximately seven times less than that of the emitter current. The resulting photo-current temperature coefficient is restricted to approximately 0.1 percent per °C. Capacitor C1 filters high frequency noise from the stage input. Integrated circuit A1 is a low drift operational amplifier used as a current to voltage converter to drive the chart recorder. Resistor R4 sets the stage output voltage to zero when the light beam to Q1 is blocked. Switch S1 controls stage gain.

Modifications made to the SD-3443-3 transistor for the present application are illustrated in Figure A-2. The glass lens was replaced by a metal plate with a 0.0254 cm (0.01 in.) pinhole. The pinhole allowed incremental viewing of the solar flux profile. The pinhole was placed as close as possible to the filter to maximize the viewing angle, where the viewing angle is defined as that angle between the peak and 50 percent response positions. However, based on laser beam measurements the modified version has only a 35° viewing angle (Fig. A-3). Also, a 0.0127 cm (0.005 in.) thick glass attenuator with a 5 percent transmittance nichrome coating was placed over the viewing port to minimize thermal loads and dust contamination. As described previously, the sensor is mounted in a conically shaped chrome coated fixture that enables water flow around the sensor, thereby maintaining constant temperature.
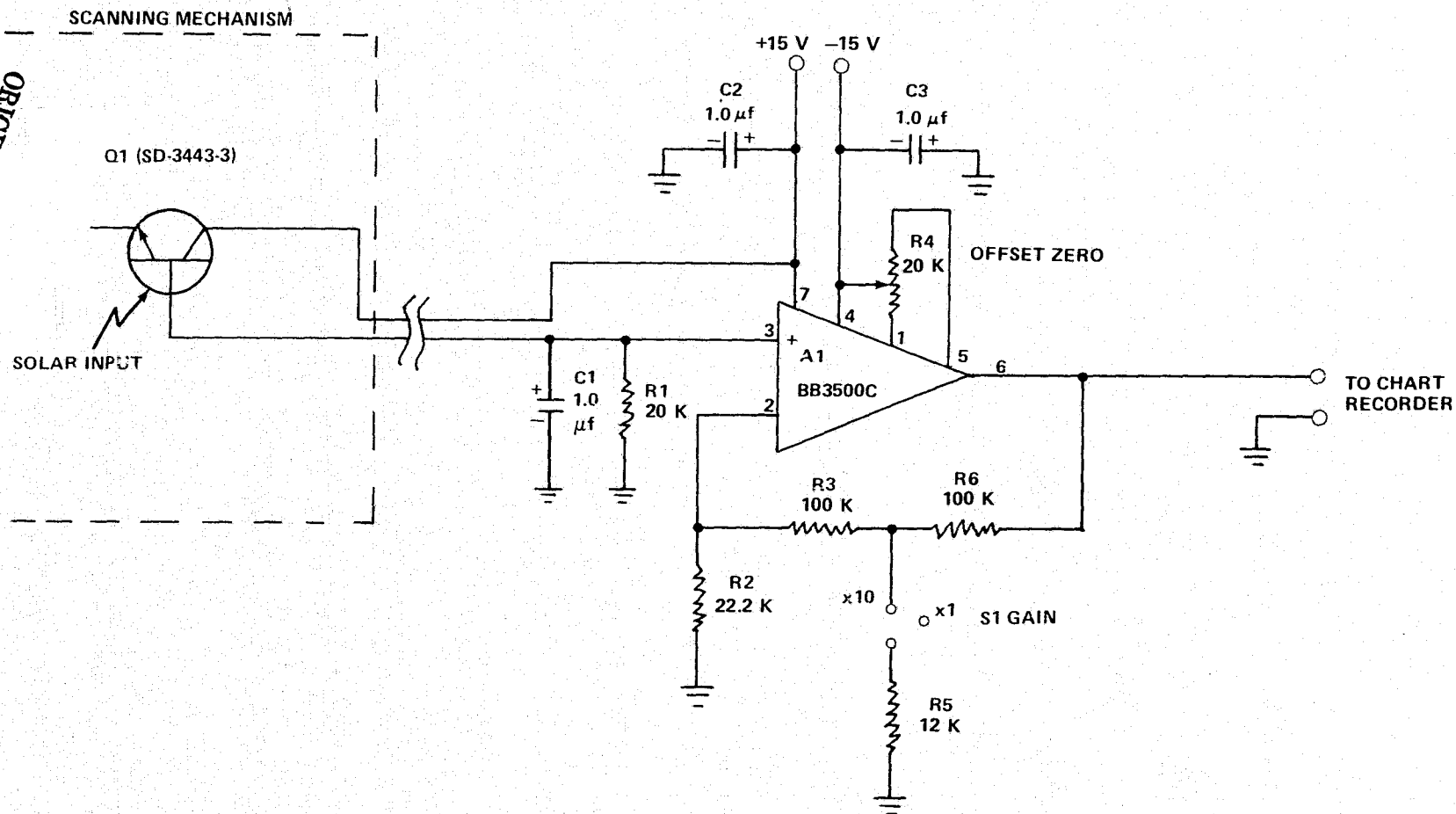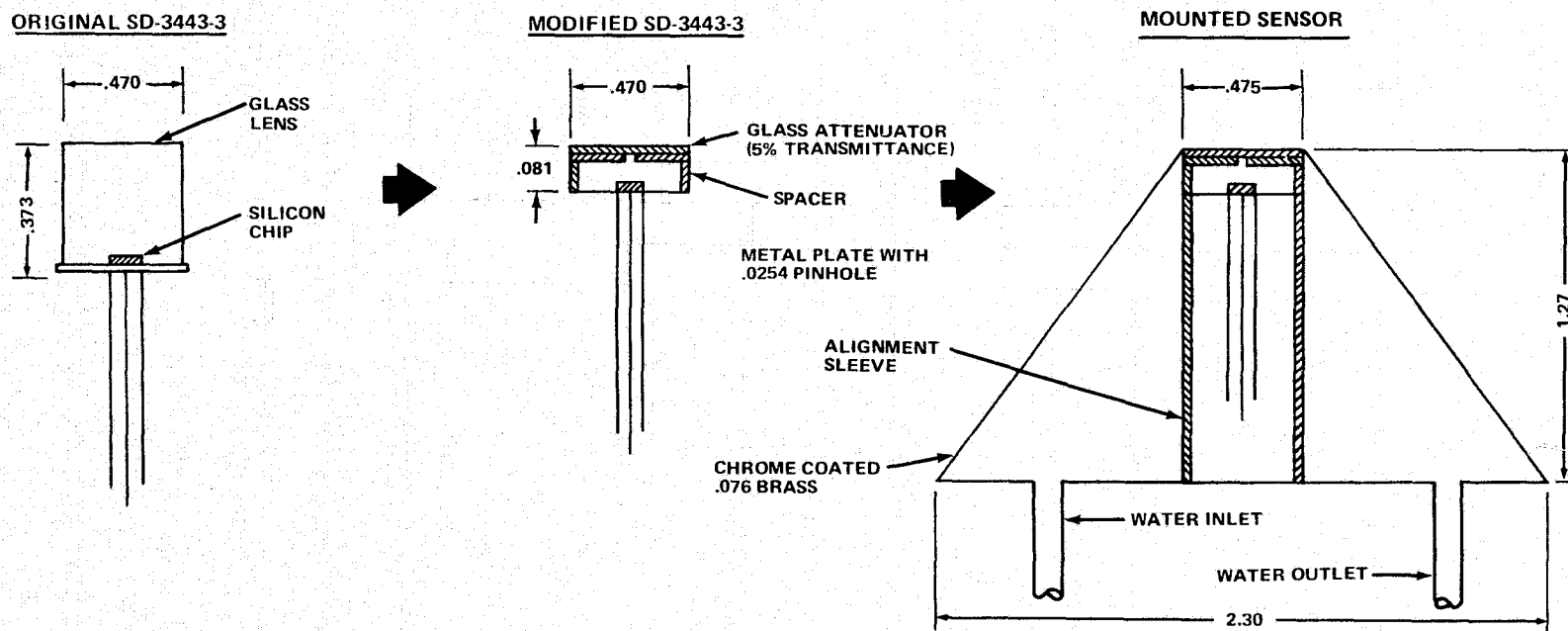
Figure A-1. Solar detector electrical diagram.

ORIGINAL SD-3443-3

.470

GLASS
LENS

.373

SILICON
CHIP

MODIFIED SD-3443-3

.470

.081

GLASS ATTENUATOR
(5% TRANSMITTANCE)

SPACER

METAL PLATE WITH
.0254 PINHOLE

MOUNTED SENSOR

.475

1.27

ALIGNMENT
SLEEVE

CHROME COATED
.076 BRASS

WATER INLET

WATER OUTLET

2.30

NOTE: ALL DIMENSIONS IN CENTIMETERS
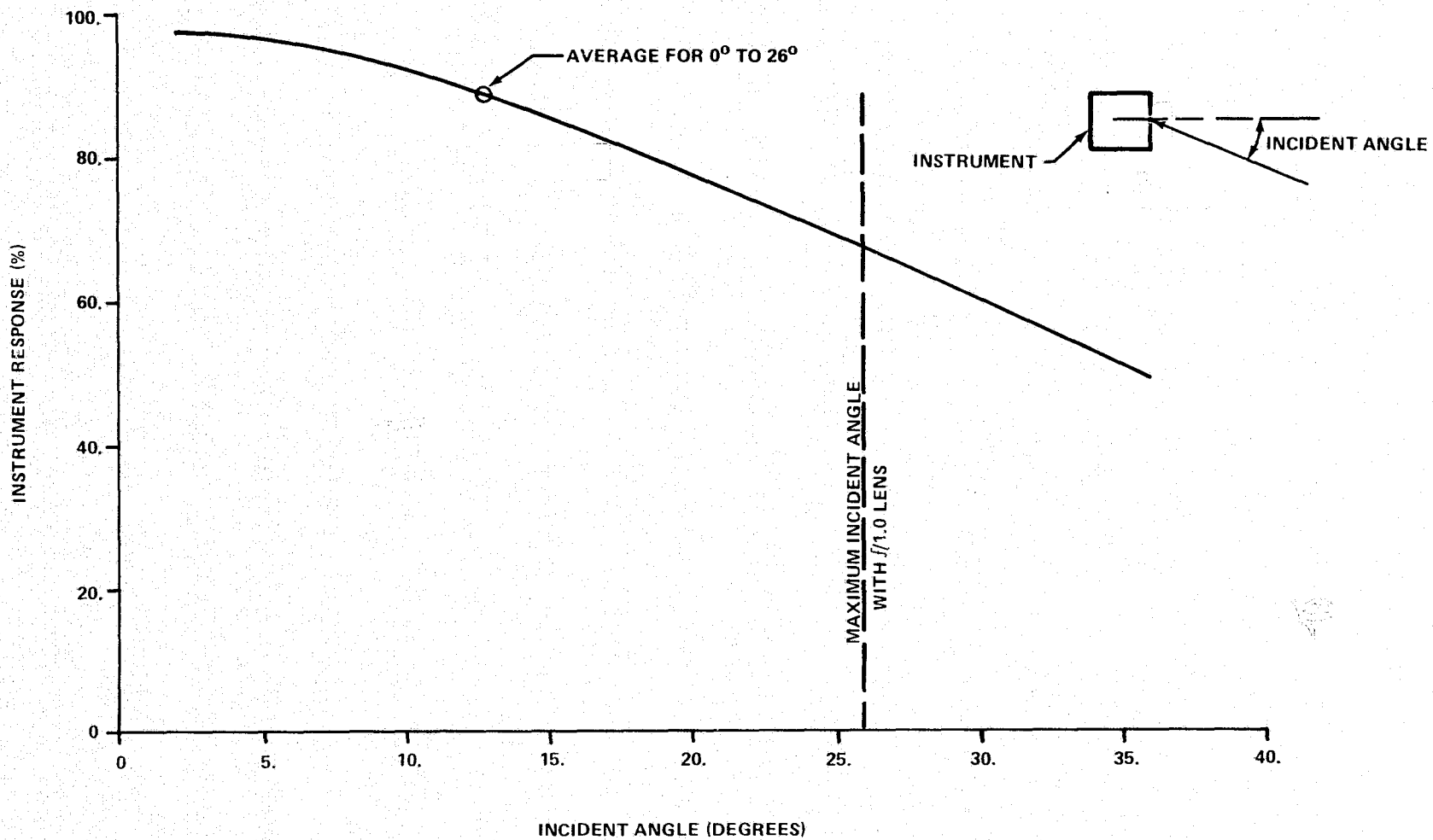
Figure A-2. Sensor SD-3443-3 physical modifications.

Figure A-3. Modified solar sensor response versus incident angle.

APPENDIX B

THERMOPILE/PHOTODIODE COMPARISON

A thermopile heat detector, Type L22 built by Sensors, Inc., was used as a baseline instrument to evaluate the adequacy of the photodiode light detector. The L22 sensor has a 0.2 by 2.0 mm active area with 20 junctions. The window material is potassium bromide with a constant transmittance over a wavelength range of 0.5 to 15 μ. The junctions were coated with organic black paint which has an invariant spectral response from 0.1 to 15 μ. Figure B-1 presents the spectral response characteristics for the photodiode and thermopile sensors.

The evaluation procedure consisted of measuring the Fresnel lens concentration characteristics with both sensors and comparing the measured data. However, utilization of the thermopile sensor was limited to concentration levels of 10 or less. Thus, the peak heat flux on the thermopile was minimized by using only 10 cm of the lens width during the sensor comparison tests.

Results of the testing were that the transmittance and peak concentration ratio indicated by the two sensors were within 1.5 and 4 percent, respectively. Since the measurements were within normal accuracy limits of the instruments, the photodiode was considered acceptable.
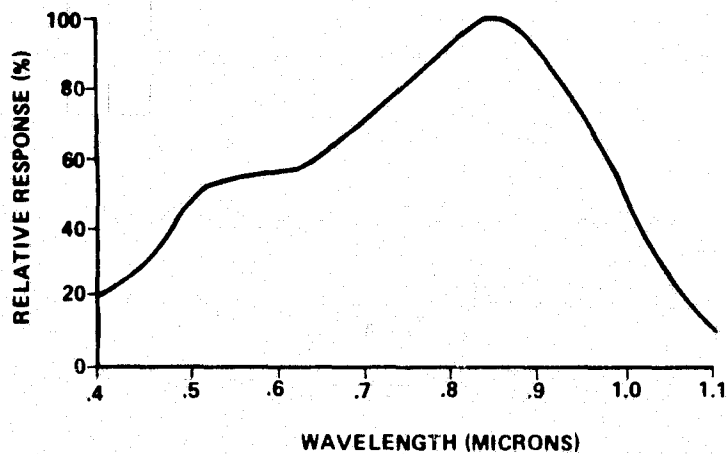
(a) SD-3443-3 SENSOR
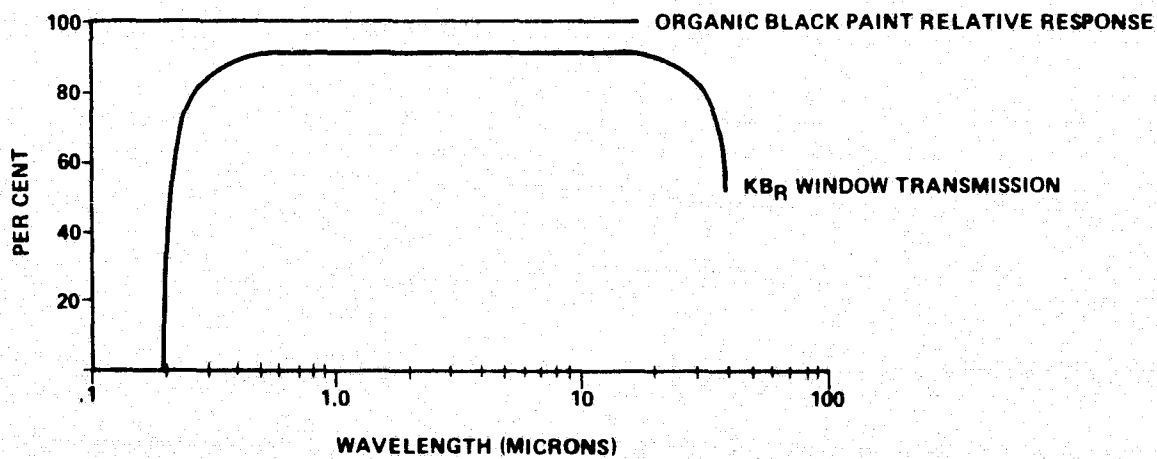
(b) L22 THERMOPILE SENSOR

Figure B-1. Solar sensor spectral response characteristics.

REFERENCES

1. Hastings, L. J.: "Experimental Evaluation of a Solar Concentrator," Proc. of First Southeastern Conference on Application of Solar Energy, Huntsville, Alabama, March 1975, pp. 333-358.

2. Cosby, R.:"Performance, Manufacture, and Protection of Large Cylindrical Fresnel Lenses for Solar Collection," Final Report, Ball State University-Marshall Space Flight Center Cooperative Agreement, Muncie, Indiana, NCA8-00103, Modification No. 2, June 1975.

3. Rainhart, L.G. and Schimmel, W.P., Jr.: "Effect of Outdoor Aging on Acrylic Sheet," SAND 74-0241, AEC Contract AT (29-1) - 789, Sandia Laboratories Energy Report, Albuquerque, New Mexico, September 1974.

4. Cosby, R.: "The Cylindrical Fresnel Lens as a Solar Concentrator," Final Report, Ball State University-Marshall Space Flight Center Cooperative Agreement, Muncie, Indiana, NCA8-00103, Modification No. 1, June 1975.

5. Born, M. and Wolf, E.: Principles of Optics, Pergamon Press, New York, Fourth Edition, 1970, pp. 38-51.

6. Moon, P.: J. Franklin Instit., vol. 23a, 1940, p. 583.

7. Rohm and Haas Company, Philadelphia, Pa., "Plexiglas Injection and Extrusion Molding Powders," Publication PL 165f, December 1968.

APPROVAL

AN ANALYTICAL AND EXPERIMENTAL EVALUATION OF A FRESNEL LENS SOLAR CONCENTRATOR
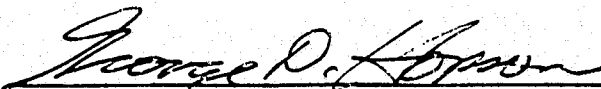
By Leon J. Hastings, Steve A. Allums, and Dr. Ronald M. Cosby

The information in this report has been reviewed for security classification. Review of any information concerning Department of Defense or Atomic Energy Commission programs has been made by the MSFC Security Classification Officer. This report, in its entirety, has been determined to be unclassified.
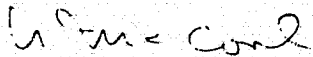
This document has also been reviewed and approved for technical accuracy.

A. F. Worlund

A. L. WORLUND
Chief, Propulsion Systems Analysis Branch

George D. Hopson

GEORGE D. HOPSON
Chief, Engineering Analysis Division

A. A. McCool

A. A. McCOOL
Director, Structures and Propulsion Laboratory